Density Functional Study on the Structure and Electronic Properties of Polycyclic Aromatic Hydrocarbons from Wildfire

Collins Adusei

Nabanita Saikia[*]

New Mexico Highlands University, Las Vegas, NM, USA

ABSTRACT

First-principles density functional theory (DFT) calculations are performed to study the effect of ring size on the structure, stability, and aromaticity of 16 polycyclic aromatic hydrocarbons (PAHs) that are listed as priority pollutants by the U.S. Environmental Protection Agency. This study aims to determine a suitable level of theory for investigating these systems. DFT functionals, namely ωB97xD, PBE-D2, B97-D3, and B3LYP, are used to compare the stability and energy gap of the PAHs. As the ring size or carbon-to-hydrogen (C/H) ratio increases, the energy gap decreases, which affects the stability, reactivity, and overall electronic energy of the PAH molecules. Nucleus-independent chemical shift calculations predict the position and number of resonant sextets or Clar structures and establish a correlation between the distribution of π-electrons in PAHs. The comparison of different functionals shows that the wB97xD functional overestimates the energy gap, whereas B3LYP performs better in predicting the energy gap with a smaller mean absolute error compared to the experimental values.

KEYWORDS: Wildfire, Polycyclic aromatic hydrocarbons, Density functional theory, Electronic properties, Energy gap, Clar structures.

1 INTRODUCTION

Forest fires pose a significant threat in the western U.S. and semi-arid/arid regions worldwide. The frequency and severity of wildfires have increased due to factors such as prolonged summer droughts, higher temperatures, earlier snowmelt, and climate change. Wildfires have significant implications for public health, as recent research has shown that minority populations, including black, Hispanic, and Native Americans, are 50% more vulnerable compared to other demographic groups (Campos and Abrantes, 2021; Davis et al., 2018). Wildfire smoke contains a mix of harmful substances, including particulate matter, toxic chemicals, gaseous substances, and semi-volatile organic compounds, such as polycyclic aromatic hydrocarbons (PAHs) (Chen et al., 2018). PAHs are produced during all combustion processes, including wildfires, and can easily enter terrestrial and aquatic ecosystems due to the susceptibility of wildfire ash to erosion (Wentworth et al., 2018; Yuan et al., 2008). The U.S. Environmental Protection Agency (EPA) has identified sixteen unsubstituted PAHs as priority pollutants found in groundwater samples, with potential links to lung, colon, and breast cancers (Srogi, 2007; Williams et al., 2013). PAHs are also byproducts of burning oil, gas, coal, fossil fuels, wood, and tobacco, as well as being emitted in cigarette smoke (Balmer et al., 2019; Kerkeni et al., 2022; McAdam et al., 2013; Vu et al., 2015).

Williams et al. (2013) reported the potential cancer risks associated with incidental ingestion of human carcinogens or B2 PAHs, including benz[a]anthracene, benzo[k]-fluoranthene, benzo[b] fluoranthene, benzo[a]pyrene, chrysene, dibenz[a,h]anthracene, and indeno[123-cd]pyrene from settled house dust and coal-tar-based pavement sealants. The exposure to B2 PAHs in settled house dust posed a significant risk for children under 6 years of age. Srogi (2007) provided a comprehensive overview of PAH concentrations in various environmental samples, such as sediment/soil, water, and air, and discussed the associated risks and hazards on the ecosystem and human health. Synthetic zeolite and clinoptilolite were used as sorbents for the removal of high-toxicity volatile organic compounds and PAHs such as anthracene, naphthalene, benzo[a]pyrene, and dibenz[a,h] anthracene in aqueous solutions (Wołowiec et al., 2017).

Computational research has investigated the interplay between PAHs and nanomaterials, indicating that nanomaterials could potentially function as cost-effective substrates for the remediation of PAH pollutants (Hu et al., 2020; Yi et al., 2022; Yue et al., 2021). The interaction between four PAH molecules (benzene, naphthalene, coronene, and ovalene) and graphene was studied using density functional theory (DFT) with empirical dispersion correction (Ershova et al., 2010). The findings revealed that an increase in the size of the PAH molecules resulted in higher binding energy and greater *z*-distance separation between the PAH molecule and the graphene surface. The frictional force for the sliding of PAH molecules on graphene increased linearly with the number of atomic contacts and was energetically favorable for a specific stacking path (Ershova et al., 2010). Dispersion-corrected DFT calculations of the adsorption of benzene, naphthalene, pyrene, chrysene, benzo[a]pyrene, coronene, and ovalene on phosphorene and graphene nanoflake showed that $\pi-\pi$ stacking of PAH-graphene was driven by dispersion forces (~60%), while electrostatic forces contributed to ~34% (Cortés-Arriagada, 2021). Moreover, PAH induced a bandgap opening in phosphorene (~10–60 meV), comparable to the bandgap opening in graphene (~10–40 meV). Despite progress in the research of PAHs at the theoretical and experimental levels (Chakarova-Käck et al., 2010; González-Berdullas and da Silva, 2021; Kerkeni et al., 2022; Liu et al., 2019; Liu et al., 2019; Ruiz-Morales, 2022), prior theoretical studies did not include all 16 PAHs listed by the U.S. EPA as priority pollutants (Chen and Wang, 2019; Kateris et al., 2023; Liu et al., 2019).

A comprehensive understanding of the arrangement of polycyclic aromatic rings within the molecular framework, as well as the structural stability, energetics, and electronic properties of PAHs, holds significance in chemistry. Our objective is to perform an in-depth theoretical investigation of PAH molecules that are relevant to the environment and to methodologically compare their structure and electronic properties. DFT calculations with empirical dispersion correction are employed to gain theoretical insights into the role of the number of polycyclic rings and the conjugation of 5- and 6-membered rings on the structure and stability of PAHs. In addition, the density of states (DOS), nucleus-independent chemical shift (NICS), and frontier molecular orbitals are computed. It is hypothesized that a methodical exploration of the structural and electronic properties of PAHs will augment our understanding of their aggregation behavior under suitable environmental conditions. This research will be particularly advantageous in elucidating the interactions of PAHs with functional nanomaterials, where intermolecular interactions are predominantly governed by weak van der Waals π–π stacking and hydrogen bonding.

2 METHODS

Sixteen PAH molecules were considered in this study (see Figure 1). Geometry optimization (minimum energy configurations) was performed in the gas phase using Becke's three-parameter Lee-Yang-Parr (B3LYP) hybrid exchange-correlation functional (Becke, 1993; Śmiga and Constantin, 2020; Stephens et al., 1994), and the double-zeta basis set 6-31G(d,p) for hydrogen and carbon atoms (Francl et al., 1982). All DFT calculations were performed using the GAUSSIAN16 program (Frisch et al., 2016). The geometry optimization was followed by a frequency calculation at the same level of theory to confirm that the geometries were in their actual ground state. The B3LYP functional combines Becke's three-parameter exchange functional and the Lee-Yang-Parr gradient-corrected correlation functional (Xu and Goddard, 2004). Though hybrid functionals are computationally more expensive than other exchange-correlation functionals, the results for ground-state properties obtained using B3LYP functional are markedly more accurate compared with experiments for systems such as PAHs in general (Ao et al., 2021; Liu et al., 2019), metal clusters (Abdalmoneam et al., 2017; Bhattacharjee et al., 2014; Contreras-Torres, 2020) and other small molecules (Ofem et al., 2022). In terms of the choice of basis set, the computed energy gap values were reported to be convergent above the 6-31G(d) basis set with absolute derivation of <1% (~0.03 eV) from the 6-311++G(d,p) basis set (Chen and Wang, 2019). Increasing the basis size from 6-31G to 6-311G or from 6-31G(d) to 6-311G(d) did not result in significant improvement in the computed energy gap (Chen and Wang, 2019).

The NICS was performed using the Gauge-Independent Atomic Orbital (GIAO-DFT) method (Ditchfield, 1974; Wolinski et al., 1990) as implemented in GAUSSIAN16. Ghost or dummy atoms were positioned at the geometrical center of each ring referred to as NICS(0) and at a distance of 1 Å above the molecular plane of the ring, referred to as NICS(1). NICS(1) is a measure of the π−electron delocalization, while NICS(0) is a gauge of the σ+π electron delocalization (Baryshnikov et al., 2013). NICS(1) indices account for the π−electronic effects. NICS calculations can identify Clar structures and the magnitude of the HOMO–LUMO energy gap can correlate to the number of resonant sextets and spatial arrangement of fused aromatic rings. It has been reported that NICS calculations are sensitive to the choice of basis set and a sufficiently large basis set can provide an accurate description of the chemical shift (Ruiz-Morales, 2004; Schleyer et al., 1996). We used the 6-31G(d,p) and 6-31+G* basis set to compare the NICS contributions of the studied PAHs with that of benzene.

Furthermore, various DFT functionals were benchmarked and geometry optimizations followed by frequency calculation were performed at different levels of theory. Grimme's empirical dispersion term was included in the geometry optimization for PBE-D2/6-31G(d,p), long-range corrected hybrid functional wB97xD/6-31G(d,p), and the semi-empirical functional B97-D3/6-31G(d,p) (Perdew et al., 1996). Due to our limited computational resources and to maintain consistency, we considered the 6-31G(d,p) basis set for all calculations to facilitate the comparison of various DFT functionals on the energetics and electronic properties of PAHs. The choice of functionals and basis sets was based on prior research (Abdalmoneam et al., 2017; Abdalmoneam et al., 2021; Saikia et al., 2016; Saikia et al., 2017; Saikia et al., 2018). Additionally, the electronic properties such as the energy gap between the highest occupied molecular orbital (HOMO) and lowest unoccupied molecular orbital (LUMO), the density of states, and the frontier molecular orbitals associated with these energy levels, were determined. Data analysis and visualization were performed using Gaussview 6.1.

3 RESULTS

3.1 Structure and Electronic Properties of the PAH

The optimized geometries of 16 PAHs are shown in Figure 1, categorized based on the number of polycyclic rings, ranging from 2 to 6. Some PAHs exhibit fused 5-membered rings, while others share the same carbon-to-hydrogen (C/H) ratio, as detailed in Table A1 of Appendix A. Notably, 5-membered rings are a constituent in many PAHs and some are situated along the edges, as observed in acenaphthylene, acenaphthene, and fluorene. The calculated average C−H and C−C bonds at the B3LYP/6-31G(d,p) level are 1.09 and 1.42 Å, respectively. Since dipole moments serve as a measure of molecular polarity, the low dipole moment values indicate that the molecules are nonpolar. All the PAHs maintain a planar geometry and exhibit low dipole moment values, except for acenaphthene, which has a dipole moment of 1.55 D. With an increase in the number of rings, the total electronic energy of the molecule decreases (becomes more negative). Among the 3-rings, those with only hexagon rings, namely anthracene and phenanthrene have lower total electronic energy values. This trend is also observed for the 4- and 5-ring PAHs.

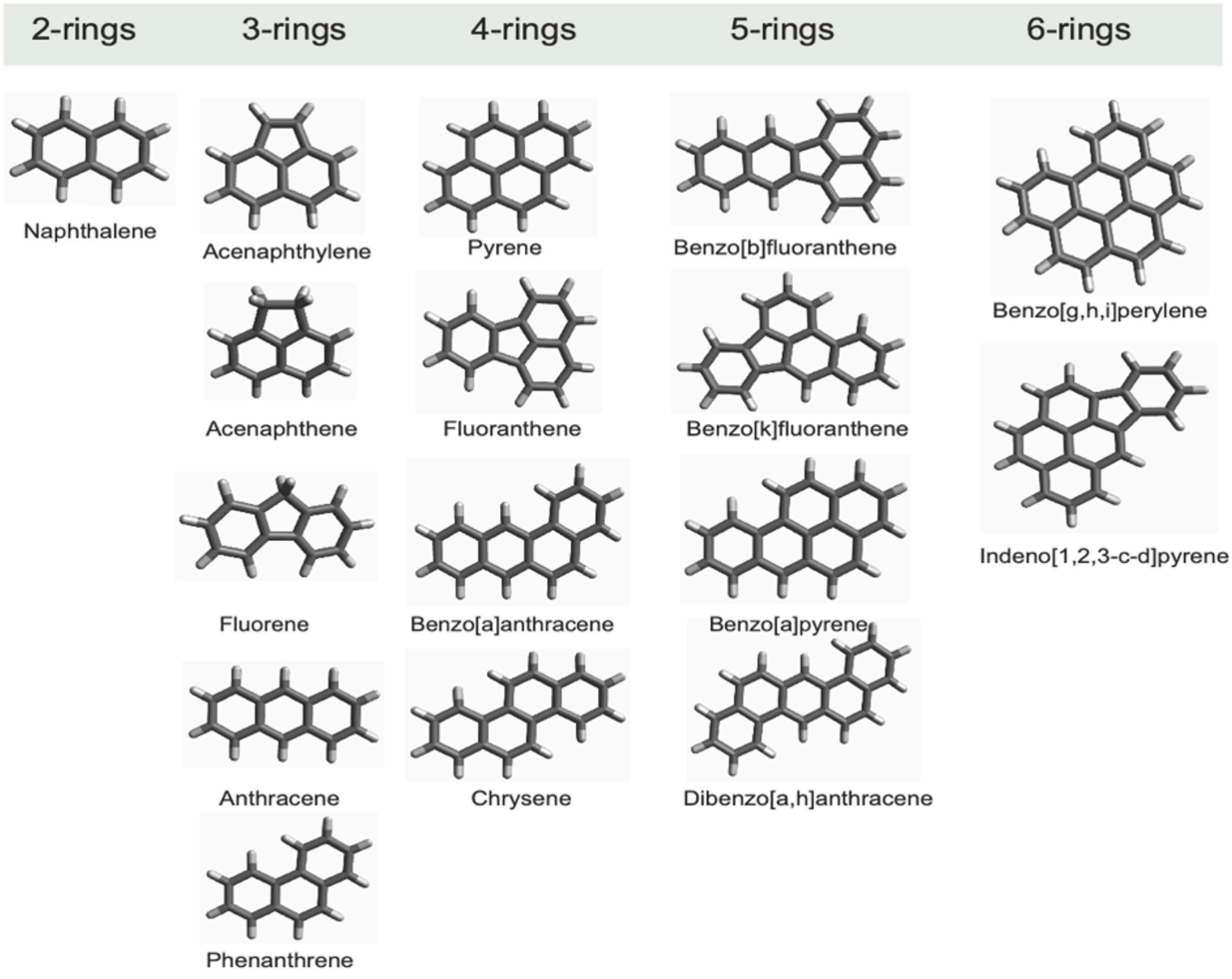

Figure 1: The gas phase optimized geometries of 16 PAHs at the B3LYP/6-31G(d,p) level. The PAHs are categorized according to their ring sizes.

The isomeric systems with the same number of atoms of each kind or C/H ratio are depicted in Figure 2, and the total electronic energy is provided in Table 1. In general, it is observed that PAHs with the same C/H ratio exhibit comparable total energy values, as evidenced by the cases of anthracene and phenanthrene; pyrene and fluoranthene; benzo[a]anthracene and chrysene; benzo[b]fluoranthene, benzo[k]fluoranthene, and benzo[a]pyrene; and benzo[g,h,i]perylene and indeno[1,2,3-c,d]pyrene.

PAH molecule	**C/H ratio**	E_{Total} **(kcal/mol)**
Anthracene	1.40	-338570.67
Phenanthrene	1.40	-338575.81
Pyrene	1.60	-386413.66
Fluoranthene	1.60	-386399.24
Benzo[a]anthracene	1.50	-434988.59
Chrysene	1.50	-434990.54
Benzo[b]fluoranthene	1.67	-482815.31
Benzo[k]fluoranthene	1.67	-482817.25
Benzo[a]pyrene	1.67	-482826.67
Benzo[g,h,i]perylene	1.83	-530668.44
Indeno[1,2,3-c,d]pyrene	1.83	-530652.63

Table 1: The total electronic energy of isomeric PAHs classified based on their C/H ratio at the B3LYP/6-31G(d,p) level.

The calculated HOMO−LUMO energy gap (E_g) at B3LYP/6-31G(d,p) level demonstrates variations with an increase in the number of polycyclic rings, as shown in Figure 3 and Table 2. Among the studied PAHs, naphthalene, comprising two aromatic rings, has an energy gap of 111.29 kcal/mol (4.83 eV). Mao et al. (2018) reported an energy gap of 4.83 eV using the B3LYP/6-31G(d,p) level, which agrees with our calculation at the same level. The optical band gap for naphthalene is reported to be 4.75 eV at the B3LYP/6-31+G(d,p) level (Costa et al., 2016), and 4.85 eV at the B3LYP/6-311G(d,p) level (Menon et al., 2019). The experimental optical band gap of naphthalene is reported to be 4.22 eV (Menon et al., 2019). Smaller PAH molecules, such as naphthalene with a higher HOMO−LUMO gap, have greater stability, rendering them less susceptible to structural degradation or modifications compared to PAHs with 4- to 6-rings.

The calculated energy gap of anthracene is 82.91 kcal/mol (3.59 eV) while the reported experimental gap is 3.27 eV (Menon et al., 2019). The experimental and computed band gap of anthracene is reported as 3.97 ± 0.22 eV and 3.37 eV, respectively (Fedorov, 2017). Using photoemission spectroscopy, Vaubel and Baessler (1968) reported an energy gap of 3.72 ± 0.03 eV. Pyrene has an energy gap of 88.58 kcal/mol (3.84 eV) at the B3LYP/6-31G(d,p) level. Malloci et al. (2007) reported a band gap of 4.45 eV for pyrene. Literature values for the band gap of pyrene are 3.78 eV (Chen and Wang, 2019), 3.75 and 3.51 eV in time−dependent DFT calculations (Kateris et al., 2023; Parac and Grimme, 2003). With empirical force fields, the band gap of pyrene was calculated to be 3.57 eV (UFF, MMFF94s) and 3.60 eV (GAFF), respectively (Kateris et al., 2023).

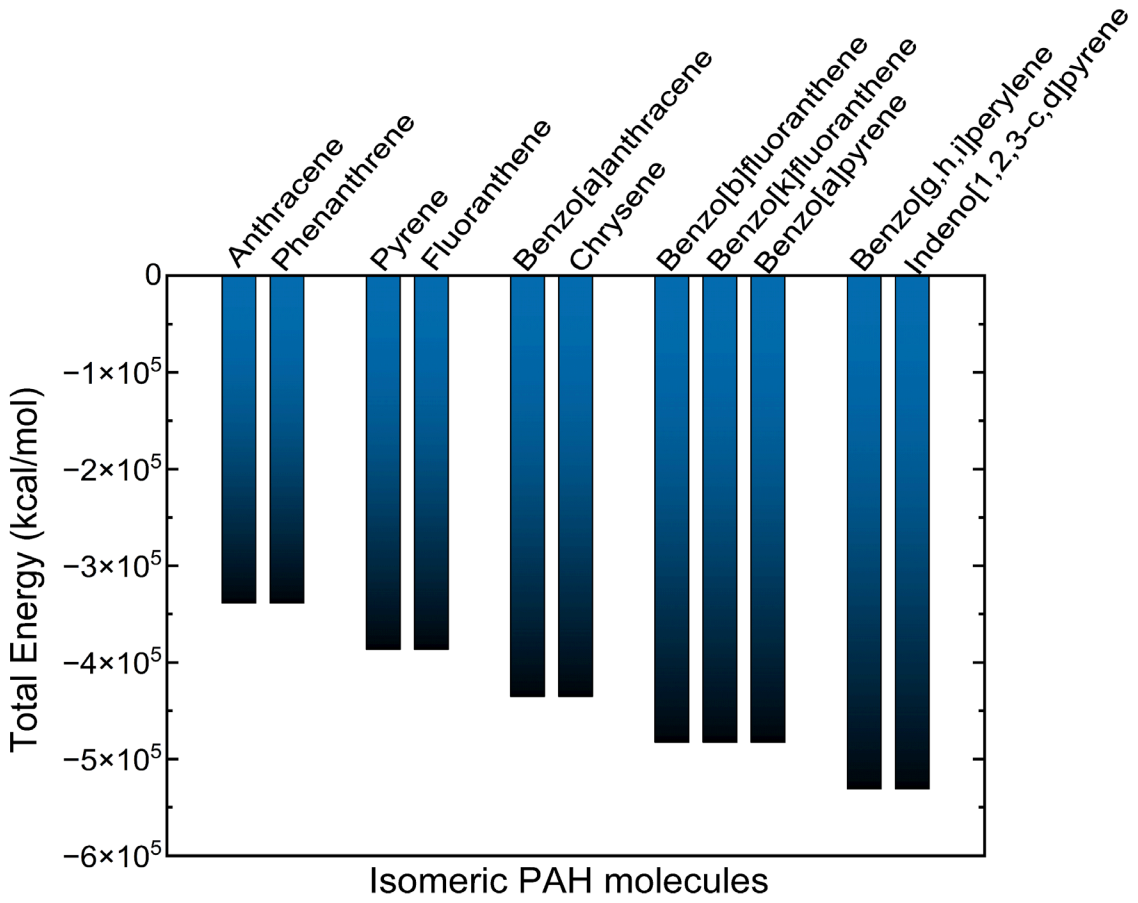

Figure 2: The total electronic energy of isomeric PAHs classified based on their C/H ratio.

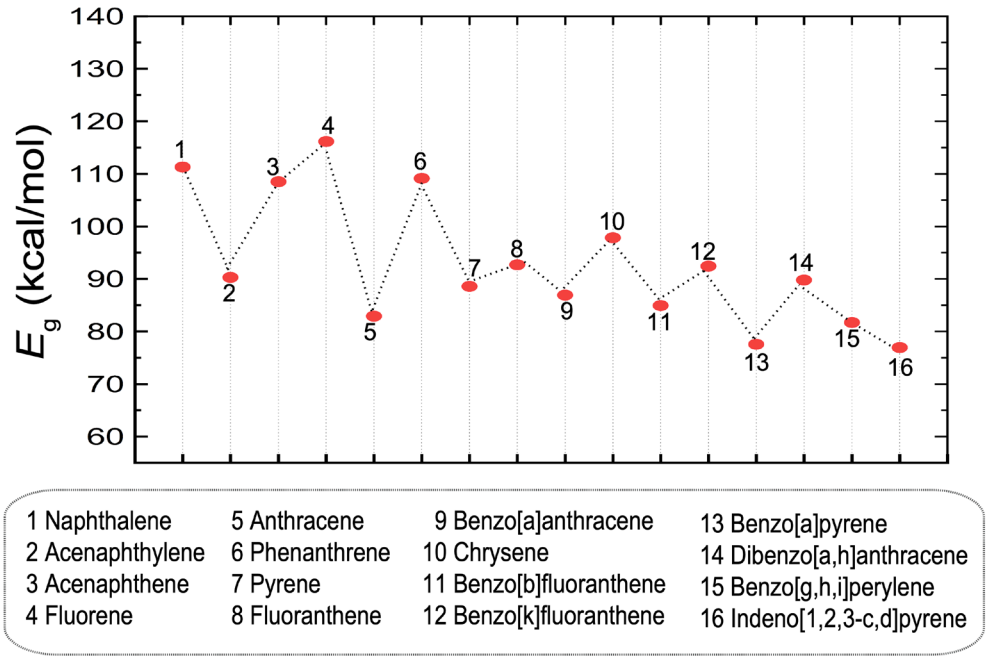

Figure 3: The HOMO−LUMO energy gap of 16 PAHs calculated at the B3LYP/6-31G(d,p) level. The energies are in units of kcal/mol.

Numbering scheme	PAH molecule	C/H ratio	E_g kcal/mol (eV)	D Debye
1	Naphthalene	1.25	111.29 (4.83)	0.0
2	Acenaphthylene	1.50	90.29 (3.92)	0.61
3	Acenaphthene	1.20	108.50 (4.70)	1.55
4	Fluorene	1.30	116.16 (5.04)	0.50
5	Anthracene	1.40	82.91 (3.59)	0.0
6	Phenanthrene	1.40	109.14 (4.73)	0.03
7	Pyrene	1.60	88.58 (3.84)	0.0
8	Fluoranthene	1.60	92.70 (4.02)	0.30
9	Benzo[a]anthracene	1.50	86.93 (3.77)	0.07
10	Chrysene	1.50	97.85 (4.24)	0.0
11	Benzo[b]fluoranthene	1.67	84.92 (3.68)	0.27
12	Benzo[k]fluoranthene	1.67	92.44 (4.01)	0.35
13	Benzo[a]pyrene	1.67	77.56 (3.36)	0.04
14	Dibenzo[a,h]anthracene	1.57	89.80 (3.89)	0.0
15	Benzo[g,h,i]perylene	1.83	81.71 (3.54)	0.05
16	Indeno[1,2,3-c,d]pyrene	1.83	76.93 (3.34)	0.61

Table 2: The C/H ratio, HOMO−LUMO energy gap, and dipole moment of the 16 PAHs at the B3LYP/6-31G(d,p) level in gas phase. The same PAH numbering scheme is used in Figure 3.

The experimental band gap of pyrene is reported to be 3.53 eV (Kateris et al., 2023). Phenanthrene, composed of three fused benzene rings has an energy gap of 109.14 kcal/mol (4.73 eV). Gümüş and Gümüş (2017) reported an energy gap of 4.74 eV at the B3LYP/6-31++G(d,p) level. The orbital energy gap of phenanthrene is reported to be 4. 78 eV (Yin et al., 2013). The energy gap of chrysene is calculated to be 97.85 kcal/mol (4.24 eV). Yang et al. (2018) reported an energy gap of 4.0 eV using the B3LYP functional. Drawing from the congruence observed between the computed HOMO−LUMO gap and existing literature on certain PAHs, we substantiate our choice of functional and basis set for this study. In general, it is noted that all PAH molecules exhibit a reduction in energy gap relative to their size, with the extent of this reduction being intricately linked to the molecular topology.

3.2. Nuclear−independent chemical shift and Clar structures

The HOMO–LUMO energy gap of PAHs is correlated with their aromaticity, specifically the number of aromatic resonant sextets or Clar's sextets (Clar, 1972; Ruiz-Morales, 2004). To comprehend the reactivity and aromaticity of PAHs, it is necessary to understand their aromatic center based on the sextet rings (Clar, 1964). In addition to the Hückel 4n+2 rule for monocyclic π–conjugated systems, the Clar sextet rule finds the resonance structure of PAHs by assigning the maximum possible number of sextets to disjoint hexagonal rings in a molecule. The presence of double bonds within an aromatic ring signifies polyene-like character in C−C bonds, and the optimal Clar structure is a closed-shell configuration with the highest number of sextet rings. The

details on the Clar sextet rule and its application to pericondensed fused benzenoid PAHs and monocyclic compounds can be found elsewhere (Alvarez-Ramírez and Ruiz-Morales, 2020; Báez-Grez et al., 2018; Ruiz-Morales, 2004).

The NICS is a magnetic−based aromaticity index that is linked to the magnetic property of a molecule and is defined as the negative value of the absolute isotropic magnetic shielding at a specified point in space. NICS(0) corresponds to the center of a ring, while NICS(1) corresponds to 1 Å above the geometrical center of a ring. The NICS is reported with a negative sign to conform with the nuclear magnetic resonance chemical shift, where positive values indicate downfield and negative values indicate upfield. A negative NICS value in the center of the ring indicates aromaticity, while a positive value denotes antiaromaticity (Ruiz-Morales, 2004; Schleyer et al., 1996).

The NICS values of PAHs calculated using GAIO−DFT are evaluated by comparing them with the NICS values of benzene at the B3LYP/6-31G(d,p) level (see Table 3 and Figures 4 and 5). Additionally, the results from the B3LYP/6-31+G* level are included, as NICS calculations are subtle to the basis set, and 6-31+G* is a recommended basis set. The results from the B3LYP/6-31+G* level are provided in Appendix B, Figures B1 and B2. The calculated NICS of benzene is consistent with previous studies (Baryshnikov et al., 2013; Ruiz-Morales, 2004). Specifically, the total NICS(0) and NICS(1) of benzene are -9.8 and -11.3 ppm at B3LYP/6-31G(d,p) level, and -8.0 and -10.1 ppm at B3LYP/6-31+G* level. Negative NICS(0) and NICS(1) values indicate the aromaticity of benzene.

Type	**$NICS_{\parallel}$**	**$NICS_{\perp}$**	**Total NICS**	**NICS anisotropy**
B3LYP/6-31G(d,p)				
NICS(0)	-7.6	-14.3	-9.8	-6.7
NICS(1)	-2.4	-29.2	-11.3	-26.8
B3LYP/6-31+G*				
NICS(0)	-5.4	-13.2	-8.0	-7.8
NICS(1)	-0.8	-28.8	-10.1	-28.0

Table 3: GIAO-DFT calculated total NICS, NICS anisotropy, $NICS_{\parallel}$ and $NICS_{\perp}$ for benzene at B3LYP/6-31G(d,p) and B3LYP/6-31+G* levels (numbers in ppm).
$NICS_{\parallel} = -(\sigma_{xx} + \sigma_{yy})/2$. $NICS_{\perp} = -\sigma_{zz}$. Total NICS = (2/3) $NICS_{\parallel}$ + (1/3) $NICS_{\perp} = -\sigma_{isotropic}$. NICS anisotropy = $NICS_{\perp} - NICS_{\parallel}$.

Figure 4 illustrates the computed NICS(0) and NICS(1) values for 2- and 3-ring PAHs at the B3LYP/6-31G(d,p) level. The NICS(0) and NICS(1) of benzene are presented for comparison, with the NICS(1) value provided in parenthesis. At a distance of 1 Å above the molecular plane, or NICS(1), the π−electron ring current is dominant, and local σ-bonding contributions diminish. The NICS of naphthalene closely resembles that of benzene, confirming the presence of two resonant sextets (10 π−electrons), with NICS(0) = -10.1 ppm and NICS(1) = -11.5 ppm for both aromatic rings of naphthalene. Acenaphthene exhibits two resonant sextets (10 π−electrons). Acenaphthylene and fluorene have 6 double bonds (12 π−electrons) but lack a resonant sextet in the hexagons. The fused 5-membered ring in acenaphthylene and fluorene yields positive NICS values, indicating an antiaromatic character at the center of the ring. Anthracene and phenanthrene each have 14 π−electrons, and the hexagons are deemed aromatic due to their negative NICS values.

The central ring of anthracene exhibits a higher NICS(0) value of -12.8 ppm compared to benzene, while for phenanthrene, the two flanking 6-membered rings have a higher NICS(0) value than benzene. A lower NICS(0) value in the central ring of phenanthrene suggests a reduced aromaticity index.

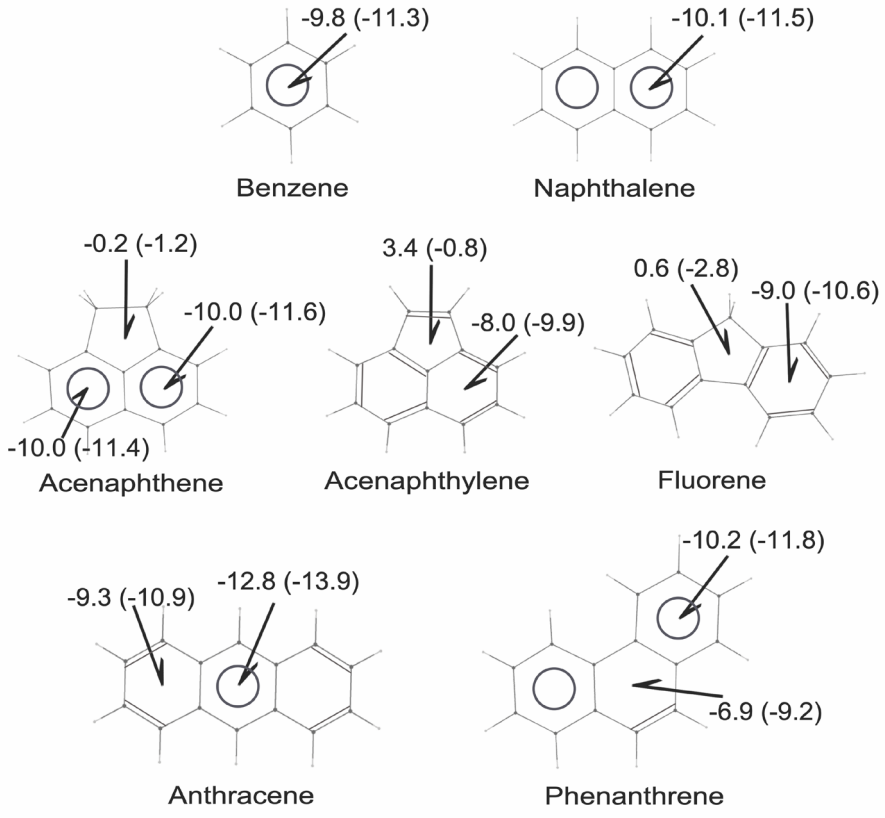

Figure 4: Structures of benzene, naphthalene, acenaphthene, acenaphthylene, fluorene, anthracene, and phenanthrene. The NICS(0) at the center of ring and NICS(1) at a distance of 1 Å above the molecular plane are presented. The NICS(1) value is shown in parentheses. The resonant sextet at the center of the ring is shown in circle.

The NICS values for PAHs containing 4-, 5-, and 6-rings are depicted in Figure 5. Pyrene with 16 π−electrons exhibits two resonant sextets and two double bonds (4 π−electrons). The NICS(0) values for the resonant sextets are higher than those of benzene, while the hexagons with two double bonds display significantly lower NICS(0) values, confirming the absence of resonant sextets in these rings. Fluoranthene, featuring a fused 5-membered ring, lacks any resonant sextets, and both NICS(0) and NICS(1) values are lower than those of benzene. The 16 π−electrons in fluoranthene behave as two disjointed conjugated systems, separated by a fused 5-membered ring. The 5-membered ring in fluoranthene exhibits a positive NICS(0) value of 4.2 ppm, indicating an antiaromatic character. Among the 4-rings PAHs, both benzo[a]anthracene and chrysene, with 18 π−electrons, possess two resonant sextets and three double bonds (6 π−electrons), with the hexagons containing the double bond displaying lower NICS values compared to benzene.

Among the 5-rings PAHs, benzo[b]fluoranthene and benzo[k]fluoranthene possess 10 double bonds, equivalent to 20 π−electrons. Benzo[b]fluoranthene lacks a resonant sextet due to its low

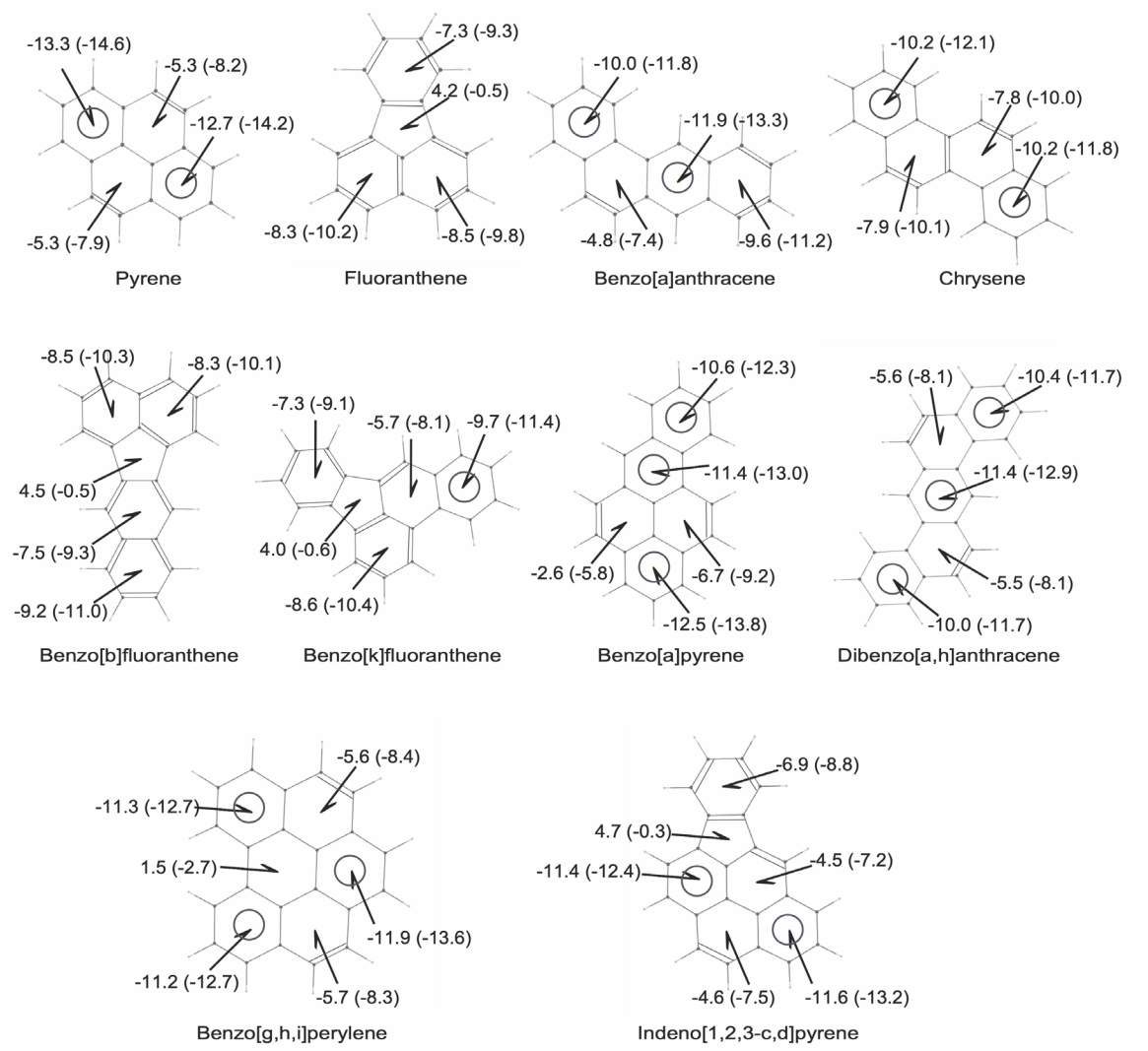

Figure 5: Structures of PAHs with four, five, and six-rings. The NICS(0) at the center of the ring and NICS(1) at a distance of 1 Å above the molecular plane are presented. The NICS(1) value is shown in parentheses. The resonant sextet that is at the center of the ring is shown in circle.

NICS value in comparison to benzene. The fused 5-membered ring in benzo[b]fluoranthene exhibits a positive NICS(0) value of 4.5 ppm, indicating an antiaromatic character. Similarly, the 5-membered ring in benzo[k]fluoranthene also displays a positive NICS(0) value, suggesting an antiaromatic character. Notably, benzo[k]fluoranthene features one resonant sextet, depicted in Figure 5, and all the hexagon rings are deemed aromatic. Benzo[a]pyrene, containing five fused hexagon rings, has 20 π−electrons, distributed among three resonant sextets and two double bonds (4 π−electrons). Dibenzo[a,h]anthracene, with 22 π−electrons, exhibits three resonant sextets and two double bonds (4 π−electrons). The aromatic character of the five hexagons in both benzo[a] pyrene and dibenzo[a,h]anthracene is evident from their negative NICS value, although two hexagons with double bonds display lower NICS values compared to benzene. In contrast, the central ring in benzo[g,h,i]perylene demonstrates an antiaromatic character with NICS(0) of 1.5 ppm. Among the five outer hexagon rings, three are resonant sextets, while the remaining two contain two double bonds (4 π−electrons). Except for the central ring, all hexagon rings in benzo[g,h,i]

perylene are aromatic. In the case of indeno[1,2,3-c,d]pyrene, the fused 5-membered ring exhibits an antiaromatic character, while the five hexagons are aromatic. Indeno[1,2,3-c,d]pyrene has 22 π−electrons, with two of the hexagons being resonant sextets and a total of 5 double bonds (10 π−electrons). Consequently, the calculated NICS values offer theoretical evidence for local aromaticity and Clar's aromatic π−sextet, thereby presenting the most significant π−conjugated, resonance structures in polycyclic aromatic systems.

All PAH molecules exhibit a decrease in the energy gap as a function of size, with the extent of the decrease being directly associated with the molecular topology. Consequently, the topology of a molecule plays a critical role in the HOMO–LUMO energy gap. Within a PAH family (with the same number of π−electron or isomeric structures), the highest number of resonant sextets corresponds to the largest HOMO–LUMO gap (Ruiz-Morales, 2004). Naphthalene, the smallest PAH has two resonant sextets. Acenaphthene with 10 π−electrons has two resonant sextets, akin to naphthalene. However, a comparison of the energy gap between acenaphthene and naphthalene indicates a higher energy gap for naphthalene possibly attributed to differences in spatial arrangement and the presence of a fused 5-membered antiaromatic ring in acenaphthene. Both acenaphthylene and fluorene have 12 π−electrons without resonant sextets. However, fluorene displays a higher energy gap than acenaphthylene. Anthracene and phenanthrene each have 14 π−electrons, yet phenanthrene features two resonant sextets, resulting in a higher energy gap. Benzo[a]anthracene and chrysene have 18 π−electrons with two resonant sextets. Still, a higher energy gap in chrysene may be attributed to the spatial arrangement of the fused benzene rings. Benzo[k]fluoranthene, with one resonant sextet, exhibits a higher energy gap compared to benzo[b]fluoranthene. Dibenzo[a,h]anthracene, benzo[g,h,i]perylene, and indeno[1,2,3-c,d]pyrene have 22 π−electrons. However, a higher energy gap in dibenzo[a,h]anthracene may be attributed to the spatial arrangement of the fused hexagon rings, with the resonant sextets occupying alternate positions.

3.3 Frontier molecular orbitals

The frontier molecular orbitals play a crucial role in elucidating the stability and chemical reactivity of molecules, as they are based on the HOMO and LUMO (Saikia and Deka, 2010; Saikia and Deka, 2011). The localization of electron density in the HOMO indicates nucleophilic sites, while the localization of LUMO suggests electrophilic sites. The frontier molecular orbitals provide insights into the overall stability, reactivity, optoelectronic properties, electrical conductivity (La Porta et al., 2012; Talipov et al., 2015; Talipov et al., 2019), and intermolecular interactions of molecules (Abdalmoneam et al., 2017; Saikia et al., 2016; Sebastianelli and Pereyra, 2020). The E_{HOMO} signifies the electron-donating ability of a molecule; with higher values indicating an increased ability to donate electrons to the unoccupied molecular orbital of a receptor. Conversely, the E_{LUMO} value is associated with the molecule's ability to accept electrons, with a lower value indicating a greater ability to accept electrons. A high HOMO–LUMO energy gap indicates greater stability and lower reactivity of the chemical species. Figure 6 illustrates the frontier molecular orbitals corresponding to the HOMO and LUMO, as well as the DOS of selected PAHs, namely naphthalene, acenaphthylene, and pyrene.

We compared the (A_u) HOMO and (B_{2g}) LUMO of naphthalene with a previous study by Yang and Bittner (2015) and observed a strong correspondence with the HOMO and LUMO isosurface. The DOS, HOMO, and LUMO of the other PAHs are provided in Appendix C. The DOS illustrates the occupied and virtual orbitals along with the energy gap. The HOMO isosurface of the three

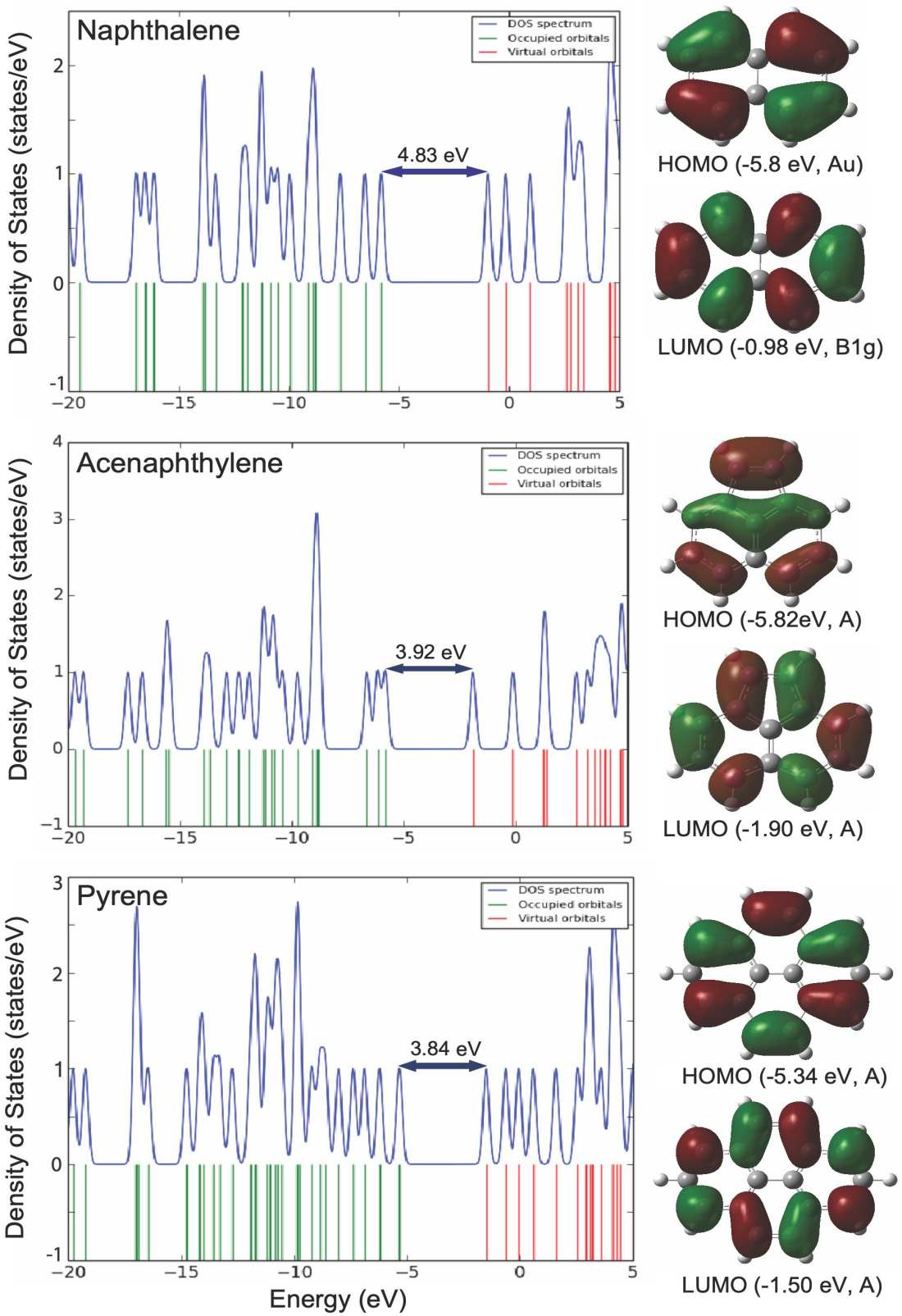

Figure 6: The DOS showing the occupied (green) and virtual (red) orbitals along with the HOMO and LUMO isosurface for naphthalene, acenaphthylene, and pyrene at the B3LYP/6-31G(d,p) level. The occupied orbital corresponds to HOMO while the virtual orbitals correspond to LUMO.

PAHs is delocalized on the C–C bond of the phenyl ring and is predominantly of π character, while the LUMO is of π* (antibonding) character and is localized on the carbon atoms of the ring with some contribution from the hydrogen atoms (see Figure 6). As shown in Table 2 and DOS plots in Figure 6, an increase in the number of polycyclic rings leads to a decrease in the HOMO–LUMO energy gap, although there are variations in the electronic energy levels even for isomeric PAHs with the same C/H ratios. This may be attributed to the presence of 5-membered rings embedded within the 6-membered rings. Overall, the energy gap calculated using DFT agrees well with previous studies (as discussed in Section 3.1 and summarized in Table 2).

3.4 Comparison of different functionals

To compare the effect of different functionals on the electronic properties of PAHs, we considered four DFT functionals and computed the HOMO–LUMO energy gap. Although the commonly utilized B3LYP hybrid functional, incorporating 20% Hartree–Fock (HF) exchange, can approximate bond lengths and vibrational frequencies in close agreement with experimental data, it does not adequately capture dispersion interactions between molecules, thus failing to accurately describe noncovalent van der Waals (vdW) interactions. This limitation becomes particularly relevant when considering the adsorption of PAHs on surfaces of nanomaterials, where weak π−π stacking interactions are prevalent (Grossman et al., 2021; Saikia et al., 2017). The Generalized Gradient Approximation using the PBE functional has been found to have deficiencies in accurately representing the self-interaction error and noncovalent vdW interactions (Saikia et al., 2017). Consequently, Grimme's empirical correction (D2) term has been incorporated into the PBE functional to address these shortcomings (Saikia et al., 2016). Grimme's D2 method effectively accounts for vdW interactions and yields comparable results at a reasonable computational cost compared to more computationally intensive methods such as CCSD(T) (Grimme, 2006; Grimme et al., 2010). The B97-D3 functional, which is a less computationally demanding dispersion-corrected functional, incorporates Grimme's functional with a Becke-Johnson damped dispersion term (Grossman et al., 2021). B97-D3, as a semi-empirical pure functional, accelerates computational efficiency for larger clusters of atoms and is reported to enhance the accuracy of vibrational analysis (Grossman et al., 2021). Range-separated functionals, such as wB97xD and hybrid exchange-correlation functional using the Coulomb-attenuating method (CAM-B3LYP), introduce a range separation parameter ω to transition between DFT and HF methods for modeling large conjugated and other systems (Chen et al., 2019; Saikia et al., 2017; Saikia et al., 2018). Notably, the wB97xD, B97-D3, and PBE-D2 functionals incorporate empirical corrections for dispersion, while B3LYP represents the level of interaction in the absence of dispersion corrections. Consequently, wB97xD, B97-D3, and PBE-D2 were compared against B3LYP energies.

Table 4 presents a comparison of the energy gap at different computational levels, namely wB97xD, PBE-D2, B3LYP, and B97-D3. The B3LYP functional demonstrates the closest agreement to the energy gap in comparison to previous studies (discussed in Section 3.1). The comparison includes the HOMO−LUMO gap and the experimentally derived optical band gap for select PAHs highlighted in bold in Table 4. The trend in the variation of the energy gap follows the order: PBE-D2 < B97-D3 < B3LYP < wB97xD which remains consistent across all 16 PAHs considered. Notably, PBE-D2 and B97-D3 underestimate the energy gap, while B3LYP and wB97xD overestimate it in comparison to experimental values. Additionally, PBE-D2 and B97-D3 exhibit comparable energy gap values.

PAH molecule (C/H ratio)	wB97xD	PBE-D2	B3LYP	B97-D3	Experiment
Naphthalene (1.25)	8.56	3.41	4.83	3.42	**4.22**[a]
Acenaphthylene (1.50)	7.726	2.47	3.91	2.50	**3.59**[a]
Acenaphthene (1.20)	8.42	3.30	4.70	2.52	-
Fluorene (1.30)	8.77	3.64	5.04	3.65	**4.06**[a]
Anthracene (1.40)	7.137	2.33	3.59	2.34	**3.27**[a] 3.97 ± 0.22[b]
Phenanthrene (1.40)	8.42	3.36	4.73	3.37	**4.16**[a]
Pyrene (1.6)	7.25	2.62	3.84	2.63	**3.64**[a]
Fluoranthene (1.6)	7.59	2.72	4.02	2.74	-
Benzo[a]anthracene (1.5)	7.31	2.51	3.77	2.52	**3.34**[a]
Chrysene (1.5)	7.82	2.94	4.24	2.95	**3.80**[a]
Benzo[b]fluoranthene (1.67)	7.19	2.43	3.68	2.45	-
Benzo[k]fluoranthene (1.67)	7.53	2.74	4.01	2.76	-
Benzo[a]pyrene (1.67)	6.73	2.20	3.36	2.22	-
Dibenzo[a,h]anthracene (1.57)	7.43	2.63	3.89	2.65	**3.3**[c]
Benzo[g,h,i]perylene (1.83)	6.91	2.37	3.54	2.38	-
Indeno[1,2,3-c,d]pyrene (1.83)	6.70	2.17	3.34	2.18	-

Table 4: HOMO−LUMO energy gap of the 16 PAHs as computed by various DFT functionals and 6-31G(d,p) basis set, given in units of eV. The optical band gap obtained from the experiment for some of the PAHs is shown in bold. (-) The experimental values are not available. [a]Menon et al., 2019; [b]Fedorov et al., 2017; [c]Zhao et al., 2022.

The HOMO–LUMO gap is utilized to interpret optical adsorption of carbon nanomaterials, although it is not a precise indicator of the optical band gap (Adkins and Miller, 2015; Adkins and Miller, 2017; Menon et al., 2019). The wB97xD functional tends to overestimate the energy gap in comparison to other functionals and experiments. Rowberg et al. (2018) reported HOMO–LUMO gaps of 7.284, 6.811, 7.602, 7.392, and 7.697 eV for anthracene, benzo[a]pyrene, benzo[b] fluoranthene, benz[a]anthracene, and chrysene, respectively, using Austin Model 1 semi-empirical quantum calculations. These values are consistent with the wB97xD functional but diverged from experimental results and other DFT functionals. Our findings, employing the wB97xD functional, agree with a previous study (Menon et al., 2019) which reported high energy gap values for naphthalene and fluorene at the wB97xD and CAM-BLYP levels of theory and a 6311G(d,p) basis set. The energy gap of naphthalene and fluorene was 8.55 eV (7.39 eV) and 8.72 eV (7.56 eV) for the wB97xD (CAM-B3LYP) functionals (Menon et al., 2019).

The mean absolute error (MAE), a statistical predictive model used to assess the average magnitude of error between calculated and experimental values, was employed to quantify the error in the HOMO–LUMO energy gap. MAE is calculated using equation 1:

$$\mathrm{MAE} = \frac{1}{n}\sum_{i=1}^{n}|y_i - \hat{y}_i| \quad (1)$$

where y_i and $\hat{y}_i$ are the energy gap calculated at the different DFT functionals and experiment and n is the number of observables.

As there is a lack of experimental data for the energy gap of certain PAHs, we performed a comparative study using various DFT functionals. MAE for wB97xD, PBE-D2, B3LYP, and B97-D3 functionals are 4.11, 0.86, 0.48, and 0.84 eV, respectively. The hybrid functional B3LYP demonstrates superior performance and a lower MAE in the computed energy gap, followed by B97-D3, PBE-D2, and wB97xD. This elucidates why B3LYP is a preferred method for accurately predicting molecular geometries and ground state properties of polycyclic aromatic systems due to its small MAE and lower computational cost. Dispersion-corrected functionals such as wB97xD may be more suitable for investigating weak interactions in which dispersion interactions are predominant.

4 DISCUSSION

The current study is centered on a systematic theoretical investigation of 16 PAHs commonly detected in environmental monitoring samples and identified as primary carcinogenic pollutants by the U.S. EPA. Calculations performed at the B3LYP/6-31G(d,p) level and benchmarked against different dispersion-corrected functionals, indicate that B3LYP has an agreement with prior theoretical calculations and experimental measurements (Costa et al., 2016; Gümüş and Gümüş, 2017; Malloci et al., 2007; Menon et al., 2019) thus supporting our choice for the theoretical calculations. The wB97xD functional which includes Grimme's dispersion correction term overestimates the energy gap of PAHs. A comparison of different DFT functionals reveals that the variation in the energy gap follows the order: PBE-D2 < B97-D3 < B3LYP < wB97xD and is consistent for all 16 PAHs. The PAH molecules exhibit a reduction in the energy gap as a function of size, with the extent of the decrease being directly associated with the molecular topology. To establish a consensus that the HOMO–LUMO gap increases with increase in number of Clar's resonant π− sextets, NICS calculations were included, and NICS(0) and NICS(1) values were compared to those of benzene. The maximum number of resonant sextets (aromaticity indices) and their localization within the aromatic ring were studied to understand the π−electron distribution in polycyclic aromatic systems. Among the studied PAHs, the maximum resonant sextets or Clar's structures were three, and the inclusion of a 5-membered ring within the PAH molecule resulted in an antiaromatic character within the 5-membered ring. Generally, for PAHs with the same number of π− electrons, the energy gap increases with an increase in the number of resonant sextets. However, if fused 5-membered rings are present, then spatial arrangement and local aromaticity must be considered. The DOS indicates the observed lowering in the energy gap and changes in the virtual and occupied orbitals along the energy gap region. The frontier molecular orbitals corresponding to HOMO are primarily delocalized on the phenyl ring and are predominantly π in character, while the LUMO is π* (antibonding) in character and is localized on the ring carbon atoms with some contribution on the hydrogen atoms.

For future research, we plan to develop a robust protocol utilizing widely employed density functionals including B3LYP-D3, BHandHYLP, PBE, PBE-D3 PBE0-D3, PBE0, M06, M06-D3, M06-L, M06-2X, M06-2X-D3, MPW1K, MPWB1K-D3, B3PW91, B3PW91-D3, B97-D, B97-D3, and CAM-B3LYP in conjunction with the 6-31G(d,p) basis set. This protocol will provide a systematic workflow for studying similar polycyclic aromatic systems. We will extend the calcu-

lations to the solvent phase to model the exposure of PAHs to water and other contaminants, as well as to explore their aggregation behavior. Furthermore, we intend to explore the potential application of graphene-based nanomaterials as effective adsorbents for all 16 PAHs in aqueous environments for detection and uptake purposes. The interaction between PAHs and nanomaterials will be governed by vdW π–π stacking interactions, and we will utilize DFT functionals such as wB97xD and PBE-D2, which are suitable for studying systems involving dispersion interactions. We anticipate that the present findings will advance the field of PAH research and offer valuable contributions to the New Mexico community through the promotion of computational research training, engagement, and involvement.

AUTHOR INFORMATION

***Corresponding Author**

Nabanita Saikia, Ph.D.
Department of Chemistry
New Mexico Highlands University
Las Vegas, NM 87701, United States
Email: nsaikia@nmhu.edu

ACKNOWLEDGMENT

The authors express their gratitude to Dr. Ian Williamson, Associate Vice President for Academic Affairs, Grants, and Contracts at New Mexico Highlands University, and the Department of Chemistry at New Mexico Highlands University for the computational support. Collins Adusei acknowledges Nicholas Adu-Effah for his contributions to the calculations and manuscript preparation. This project is supported by the FRC research seed grant from New Mexico Highlands University.

REFERENCES

Abdalmoneam, M. H.; Waters, K.; Saikia, N.; Pandey, R. Amino-Acid-Conjugated Gold Clusters: Interaction of Alanine and Tryptophan with Au_8 and Au_{20}. *J. Phys. Chem. C* **2017**, *121* (45), 25585–25593. DOI: 10.1021/acs.jpcc.7b09108.

Abdalmoneam, M. H.; Saikia, N.; Abd El-Mageed, H. R.; Pandey, R. First principles study of the optical response of Au_8 cluster conjugated with methionine, tryptophan, and tryptophyl-methionine dipeptide. *J. Phys. Org. Chem*. **2021**, *34* (7), e4201. DOI: 10.1002/poc.4201.

Adkins, E. M.; Miller, J. H. Extinction Measurements for Optical Band Gap Determination of Soot in a series of Nitrogen-Diluted Ethylene/Air Non-Premixed Flames. *Phys. Chem. Chem. Phys*. **2015**, *17* (4), 2686–2695. DOI: 10.1039/c4cp04452e.

Adkins, E. M.; Miller, J. H. Towards a Taxonomy of Topology for Polynuclear Aromatic Hydrocarbons: Linking Electronic and Molecular Structure. *Phys. Chem. Chem. Phys*. **2017**, *19* (41), 28458–28469. DOI: 10.1039/c7cp06048c.

Alvarez-Ramírez, F.; Ruiz-Morales, Y. Database of Nuclear Independent Chemical Shifts (NICS) versus NICS(ZZ) of Polycyclic Aromatic Hydrocarbons (PAHs). *J. Chem. Inf. Model.* **2020**, *60* (2), 611–620. DOI: 10.1021/acs.jcim.9b00909.

Ao, C.; Ruan, S.; He, W.; Liu, Y.; He, C.; Xu, K.; Zhang, L. Toward High-level Theoretical Studies on the Reaction Kinetics of PAHs Growth Based on HACA Pathway: An ONIOM[G3(MP2,CC)//B3LYP:DFT] Method Developed. *Fuel* **2021**, *301*, 121052. DOI: 10.1016/j.fuel.2021.121052.

Báez-Grez, R.; Ruiz, L.; Pino-Rios, R.; Tiznado, W. Which NICS Method is Most Consistent with Ring Current Analysis? Assessment in Simple Monocycles. *RSC Adv.* **2018**, *8* (24), 13446–13453. DOI: 10.1039/c8ra01263f.

Balmer, J. E.; Hung, H.; Yu, Y.; Letcher, R. J.; Muir, D. C. G. Sources and Environmental Fate of Pyrogenic Polycyclic Aromatic Hydrocarbons (PAHs) in the Arctic. *Emerging Contaminants* **2019**, *5*, 128-142. DOI: 10.1016/j.emcon.2019.04.002.

Baryshnikov, G. V.; Minaev, B. F.; Pittelkow, M.; Nielsen, C. B.; Salcedo, R. Nucleus-independent Chemical Shift Criterion for Aromaticity in π-extended Tetraoxa[8]circulenes. *J. Mol. Model.* **2013**, *19* (2), 847–850. DOI: 10.1007/s00894-012-1617-7.

Becke, A. D. Density-functional Thermochemistry. III. The Role of Exact Exchange. *J. Chem. Phys*. **1993**, *98*, 5648–5652. DOI: 10.1063/1.464913.

Bhattacharjee, D.; Mishra, B. Kr.; Chakrabartty, A. Kr.; Deka, R. Ch. DFT and QTAIM Studies on Structure and Stability of Beryllium Doped Gold Clusters. *Comput. Theor. Chem.* **2014**, *1034*, 61–72. DOI: 10.1016/j.comptc.2014.02.007.

Campos, I.; Abrantes, N. Forest Fires as Drivers of Contamination of Polycyclic Aromatic Hydrocarbons to the Terrestrial and Aquatic Ecosystems. *Curr. Opin. Environ. Sci. Health* **2021**, *24*, 100293. DOI: 10.1016/j.coesh.2021.100293.

Chakarova-Käck, S. D.; Vojvodic, A.; Kleis, J.; Hyldgaard, P.; Schröder, E. Binding of Polycyclic Aromatic Hydrocarbons and Graphene Dimers in Density Functional Theory. *New J. Phys.* **2010**, *12* (1), 013017. DOI: 10.1088/1367-2630/12/1/013017.

Chen, H.; Chow, A. T.; Li, X.-W.; Ni, H.-G.; Dahlgren, R. A.; Zeng, H.; Wang, J.-J. Wildfire Burn Intensity Affects the Quantity and Speciation of Polycyclic Aromatic Hydrocarbons in Soils. *ACS Earth Space Chem.* **2018**, 2 (12), 1262–1270. DOI: 10.1021/acsearthspacechem.8b00101.

Chen, D.; Wang, H. HOMO–LUMO Gaps of Homogeneous Polycyclic Aromatic Hydrocarbon Clusters. *J. Phy. Chem. C* **2019**, *123* (45), 27785–27793. DOI: 10.1021/acs.jpcc.9b08300.

Chen, D.; Wang, H. HOMO-LUMO Energy Splitting in Polycyclic Aromatic Hydrocarbons and their Derivatives. *Proceed. Combust. Inst.* **2019**, *37* (1), 953–959. DOI: 10.1016/j.proci.2018.06.120.

Chen, Z.; Li, Y.; He, Z.; Xu, Y.; Yu, W.-H. Theoretical Investigations on Charge Transport Properties of Tetrabenzo[a,d,j,m]coronene Derivatives using Different Density Functional Theory Functionals (B3LYP, M06-2X, and wB97XD). *J. Chem. Res.* **2019**, *43*(7-8), 293–303. DOI: 10.1177/1747519819861626.

Clar, E. Polycyclic Hydrocarbons; Academic Press: London, 1964.

Clar, E. The Aromatic Sextet; Wiley-Interscience: London, 1972.

Contreras-Torres, F. F. Dispersion-Corrected Density Functional Theory Study of the Noncovalent Complexes Formed with Imidazo[1,2-a]pyrazines Adsorbed onto Silver Clusters. *ACS Omega* **2020**, *5* (1), 561–569. DOI: 10.1021/acsomega.9b03127.

Cortés-Arriagada, D. High Stability and Properties of Adsorbed Polycyclic Aromatic Hydrocarbons (PAHs) onto Phosphorene: An Atomistic DFT Study. *J. Mol. Liq.* **2021**, *341*, 117465. DOI: 10.1016/j.molliq.2021.117465.

Costa, J. C. S.; Taveira, R. J. S.; Lima, C. F. R. A. C.; Mendes, A.; Santos, L. M. N. B. F. Optical Band Gaps of Organic Semiconductor Materials. *Opt. Mater.* **2016**, *58*, 51–60. DOI: 10.1016/j.optmat.2016.03.041.

Davies, I. P.; Haugo, R. D.; Robertson, J. C.; Levin, P. S. The Unequal Vulnerability of Communities of Color to Wildfire. *PLoS One* **2018**, *13* (11), e0205825. DOI: 10.1371/journal.pone.0205825.

Ditchfield, R. Self-Consistent Perturbation Theory of Diamagnetism. *Mol. Phys*. **1974**, *27* (4), 789–807. DOI: 10.1080/00268977400100711.

Ershova, O. V.; Lillestolen, T. C.; Bichoutskaia, E. Study of Polycyclic Aromatic Hydrocarbons Adsorbed on Graphene using Density Functional Theory with Empirical Dispersion Correction. *Phys. Chem. Chem. Phys.* **2010**, *12*, 6483–6491. DOI: 10.1039/C000370K.

Fedorov, I. A. First-Principles Study of Band Structures of Anthracene and Tetracene under Pressure. *Mater. Chem. Phys.* **2017**, *199*, 173–178. DOI: 10.1016/j.matchemphys.2017.06.060.

Francl, M. M.; Pietro, W. J.; Hehre, W. J.; Binkley, J. S.; Gordon, M. S.; DeFrees, D. J. Pople, J. A. Self-Consistent Molecular Orbital Methods. XXIII. A Polarization-Type Basis Set for Second-Row Elements. *J. Chem. Phys.* **1982**, *77* (7), 3654−3665. DOI: 10.1063/1.444267.

Frisch, M. J.; Trucks, G. W.; Schlegel, H. B.; Scuseria, G. E.; Robb, M. A.; Cheeseman, J. R.; Scalmani, G.; Barone, V.; Mennucci, B.; Petersson, G. A., et. al. Gaussian 16, Revision C.01, Gaussian Inc., Wallingford CT, 2016.

Grimme, S. Semiempirical GGA-Type Density Functional Constructed with a Long-Range Dispersion Correction. *J. Comput. Chem*. **2006**, *27* (15), 1787−1799. DOI: 10.1002/jcc.20495.

Grimme, S.; Antony, J.; Ehrlich, S.; Krieg, H. A Consistent and Accurate ab initio Parametrization of Density Functional Dispersion Correction (DFT-D) for the 94 Elements H-Pu. *J. Chem. Phys.* **2010**, *132*, 154104. DOI: 10.1063/1.3382344.

González-Berdullas, P.; da Silva, L. P. TD-DFT Monitoring of the Absorption Spectra of Polycyclic Aromatic Hydrocarbons over the Basque Country, Spain. *Sustain. Chem*. **2021**, *2* (4), 599-609. DOI: 10.3390/suschem2040033.

Grossman, E. F.; Daramola, D. A.; Botte, G. G. Comparing B3LYP and B97 Dispersion-Corrected Functionals for Studying Adsorption and Vibrational Spectra in Nitrogen Reduction. *ChemistryOpen* **2021**, *10* (3), 316–326. DOI: 10.1002/open.202000158.

Gümüş, S.; Gümüş, A. A Computational Study on a Series of Phenanthrene and Phenanthroline Based Potential Organic Photovoltaics. *Macedonian J. Chem. Chem. Eng.* **2017**, *36* (2), 239–249. DOI:10.20450/mjcce.2017.1199.

Hu, B.; Gao, Z.; Wang, H.; Wang, J.; Cheng, M. Computational Insights into the Sorption Mechanism of Polycyclic Aromatic Hydrocarbons by Carbon Nanotube through Density Functional Theory Calculation and Molecular Dynamics Simulation. *Comput. Mater. Sci.* **2020**, *179*, 109677. DOI: 10.1016/j.commatsci.2020.109677.

Kateris, N.; Jayaraman, A. S.; Wang, H. HOMO-LUMO Gaps of Large Polycyclic Aromatic Hydrocarbons and their Implication on the Quantum Confinement Behavior of Flame-Formed Carbon Nanoparticles. *Proceed. Combust. Inst.* **2023**, *39* (1), 1069-1077. DOI: 10.1016/j.proci.2022.07.168.

Kerkeni, B.; García-Bernete, I.; Rigopoulou, D.; Tew, D. P.; Roche, P. F.; Clary, D. C. Probing Computational Methodologies in Predicting Mid-Infrared Spectra for Large Polycyclic Aromatic Hydrocarbons. *Monthly Notices of the Royal Astronomical Society* **2022**, *513* (3), 3663–3681. DOI: 10.1093/mnras/stac976.

La Porta, F.; Giacoppo, J.; Ramos, P. H.; Guerreiro, M. C.; Ramalho, T. C. Computational Insights into the Role of the Frontiers Orbital in the Chemistry of Tridentate Ligands. *Am. J. Anal. Chem.* **2012**, *2* (5), 255–262. DOI: 10.5923/j.chemistry.20120205.03.

Liu, C.; Singh, A. V.; Saggese, C.; Tang, Q.; Chen, D.; Wan, K.; Vinciguerra, M.; Commodo, M.; De Falco, G.; Minutolo, P.; D'Anna, A.; Wang, H. Flame-Formed Carbon Nanoparticles Exhibit Quantum Dot Behaviors. *Proc. Natl. Acad. Sci. U S A.* **2019**, *116* (26), 12692–12697. DOI: 10.1073/pnas.1900205116.

Liu, P.; Zhang, Y.; Li, Z.; Bennett, A.; Lin, H.; Sarathy, S. M.; Roberts, W. L. Computational Study of Polycyclic Aromatic Hydrocarbons Growth by Vinylacetylene Addition. *Combust. & Flame* **2019**, *202*, 276–291. DOI: 10.1016/j.combustflame.2019.01.023.

Liu, P.; Li, Z.; Roberts, W. L. The Growth of PAHs and Soot in the Post-Flame Region. *Proceed. Combust. Inst.* **2019**, *37* (1), 977–984. DOI: 10.1016/j.proci.2018.05.047.

Malloci, G.; Mulas, G.; Cappellini, G.; Joblin, C. Time-Dependent Density Functional Study of the Electronic Spectra of Oligoacenes in the Charge States −1, 0, +1, and +2. *Chem. Phys.* **2007**, *340* (1-3), 43–58. DOI: 10.1016/j.chemphys.2007.07.046.

Mao, Y.; Head-Gordon, M.; Shao, Y. Unraveling Substituent Effects on Frontier Orbitals of

Conjugated Molecules using an Absolutely Localized Molecular Orbital Based Analysis. *Chem. Sci.* **2018**, *9* (45), 8598–8607. DOI: 10.1039/c8sc02990c.

McAdam, K. G.; Faizi, A.; Kimpton, H.; Porter, A.; Rodu, B. Polycyclic Aromatic Hydrocarbons in US and Swedish Smokeless Tobacco Products. *Chem. Central J.* **2013**, *7*, 151. DOI: 10.1186/1752-153X-7-151.

Menon, A.; Dreyer, J. A. H.; Martin, J. W.; Akroyd, J.; Robertson, J.; Kraft, M. Optical Band Gap of Cross-Linked, Curved, and Radical Polyaromatic Hydrocarbons. *Phys. Chem. Chem. Phys.* **2019**, *21* (29), 16240–16251. DOI: 10.1039/c9cp02363a.

Ofem, M. I.; Louis, H.; Agwupuye, J. A.; Ameuru, U. S.; Apebende, G. C.; Gber, T. E.; Odey, J. O.; Musa, N.; Ayi, A. A. Synthesis, Spectral Characterization, and Theoretical Investigation of the Photovoltaic Properties of (E)-6-(4-(dimethylamino)phenyl)diazenyl)-2-octyl-benzoisoquinoline-1, 3-dione. *BMC Chem.* **2022**, *16* (1), 109. DOI: 10.1186/s13065-022-00896-w.

Parac, M.; Grimme, S. A TDDFT Study of the Lowest Excitation Energies of Polycyclic Aromatic Hydrocarbons. *Chem. Phys.* **2003**, *292* (1), 11–21. DOI: 10.1016/s0301-0104(03)00250-7.

Perdew, J. P.; Burke, K.; Wang, Y. Generalized Gradient Approximation for the Exchange-Correlation Hole of a Many-Electron System. *Phys. Rev. B Condens. Matter* **1996**, *54* (23), 16533–16539. DOI: 10.1103/physrevb.54.16533.

Rowberg, K.; Nataraj, N.; Saroian, W.; Kang, L. Theoretical Evaluation of Substituted Polycyclic Aromatic Hydrocarbons as Emerging Pollutant Phototoxins. *WIT Trans. Ecol. Environ.* **2008**, *111*, 329–337. DOI: 10.2495/WP080321.

Ruiz-Morales, Y. The Agreement between Clar Structures and Nucleus-Independent Chemical Shift Values in Pericondensed Benzenoid Polycyclic Aromatic Hydrocarbons: An Application of the Y-Rule. *J. Phys. Chem. A* **2004**, *108* (49), 10873–10896. DOI: 10.1021/jp040179q.

Ruiz-Morales, Y. Application of the Y-Rule and Theoretical Study to Understand the Topological and Electronic Structures of Polycyclic Aromatic Hydrocarbons from Atomic Force Microscopy Images of Soot, Coal Asphaltenes, and Petroleum Asphaltenes. *Energy Fuels* **2022**, *36* (16), 8725–8748. DOI: 10.1021/acs.energyfuels.2c01170.

Saikia, N.; Deka, R. C. Theoretical Study on Pyrazinamide Adsorption onto Covalently Functionalized (5,5) Metallic Single-Walled Carbon Nanotube. *Chem. Phys. Lett.* **2010**, *500* (1-3), 65–70. DOI: 10.1016/j.cplett.2010.09.075.

Saikia, N.; Deka, R. C. Density Functional Calculations on Adsorption of 2-methylheptylisonicotinate Antitubercular Drug onto Functionalized Carbon Nanotube. *Comput. Theor. Chem.* **2011**, *964* (1-3), 257–261. DOI: 10.1016/j.comptc.2011.01.006.

Saikia, N.; Seel, M.; Pandey, R. Stability and Electronic Properties of 2D Nanomaterials Conjugated with Pyrazinamide Chemotherapeutic: A First-Principles Cluster Study. *J. Phys. Chem. C* **2016**, *120* (36), 20323–20332. DOI: 10.1021/acs.jpcc.6b06000.

Saikia, N.; Karna, S. P.; Pandey, R. Theoretical Study of Gas and Solvent Phase Stability and Molecular Adsorption of Noncanonical Guanine Bases on Graphene. *Phys. Chem. Chem. Phys.* **2017**, 19 (25), 16819–16830. DOI: 10.1039/c7cp02944f.

Saikia, U.; Saikia, N.; Waters, K.; Pandey, R.; Sahariah, M. B. Electronic Properties of Acetaminophen Adsorbed on 2D Clusters: A First Principles Density Functional Study. *ChemistrySelect* **2017**, *2* (13), 3613–3621. DOI: 10.1002/slct.201601593.

Saikia, N.; Johnson, F.; Waters, K.; Pandey, R. Dynamics of Self-Assembled Cytosine Nucleobases on Graphene. *Nanotechnol*. **2018**, *29* (19), 195601. DOI: 10.1088/1361-6528/aab0ea.

Schleyer, P. V. R.; Maerker, C.; Dransfeld, A.; Jiao, H.; Hommes, N. J. R. V. E. Nucleus-Independent Chemical Shifts: A Simple and Efficient Aromaticity Probe. *J. Am. Chem. Soc.* **1996**, *118* (26), 6317–6318. DOI: doi: 10.1021/ja960582d.

Sebastianelli, P.; Pereyra, R. G. Frontier Molecular Orbital Analysis for Determining the Equilibrium Geometries of Atmospheric Prenucleation Complexes. *Int. J. Quant. Chem.* **2020**, *120* (3), e26060. DOI: 10.1002/qua.26060.

Śmiga, S.; Constantin, L. A. Unveiling the Physics Behind Hybrid Functionals. *J. Phys. Chem. A* **2020**, *124* (27), 5606–5614. DOI: 10.1021/acs.jpca.0c04156.

Srogi, K. Monitoring of Environmental Exposure to Polycyclic Aromatic Hydrocarbons: A Review. *Environ. Chem. Lett.* **2007**, *5* (4), 169–195. DOI: 10.1007/s10311-007-0095-0.

Stephens, P. J.; Devlin, F. J.; Chabalowski, C. F.; Frisch, M. J. Ab Initio Calculation of Vibrational Absorption and Circular Dichroism Spectra Using Density Functional Force Fields. *J. Phys. Chem*. **1994**, *98* (45), 11623–11627. DOI: 10.1021/j100096a001.

Talipov, M. R.; Boddeda, A.; Lindeman, S. V.; Rathore, R. Does Koopmans' Paradigm for 1-Electron Oxidation Always Hold? Breakdown of IP/E_{ox} Relationship for p-Hydroquinone Ethers and the Role of Methoxy Group Rotation. *J. Phys. Chem. Lett.* **2015**, *6* (17), 3373–3378. DOI: 10.1021/acs.jpclett.5b01532.

Talipov, M. R.; Navale, T. S.; Rathore, R. The HOMO Nodal Arrangement in Polychromophoric Molecules and Assemblies Controls the Interchromophoric Electronic Coupling. *Angew. Chem. Int. Ed. Engl.* **2015**, *54* (48), 14468–14472. DOI: 10.1002/anie.201506402.

Talipov, M. R.; Steiner, E. Coexistence of Structurally Similar but Electronically Distinct Isomers of Delocalized Cation Radicals as a Basis for the Development of Functional Materials. *Phys. Chem. Chem. Phys.* **2019**, *21* (20), 10738–10743. DOI: 10.1039/c9cp02271f.

Vaubel, G.; Baessler, H. Determination of the Band-Gap in Anthracene. *Phys. Lett. A.* **1968**, *27* (6), 328–329. DOI: 10.1016/0375-9601(68)91032-3.

Vu, A. T.; Taylor, K. M.; Holman, M. R.; Ding, Y. S.; Hearn, B.; Watson, C. H. Polycyclic Aromatic Hydrocarbons in the Mainstream Smoke of Popular U.S. Cigarettes. *Chem. Res. Toxicol.* **2015**, *28* (8), 1616–1626. DOI: 10.1021/acs.chemrestox.5b00190.

Wentworth, G. R.; Aklilu, Y.-A.; Landis, M. S.; Hsu, Y.-M. Impacts of a Large Boreal Wildfire on Ground Level Atmospheric Concentrations of PAHs, VOCs and Ozone. *Atmos. Environ.* (1994). **2018**, *178*, 19–30. DOI: 10.1016/j.atmosenv.2018.01.013.

Williams, E. S.; Mahler, B. J.; Van Metre, P. C. Cancer Risk from Incidental Ingestion Exposures to PAHs Associated with Coal-Tar-Sealed Pavement. *Environ. Sci. Technol.* **2013**, *47* (2), 1101–1109. DOI: 10.1021/es303371t.

Wolinski, K.; Hinton, J. F.; Pulay, P. Efficient Implementation of the Gauge-Independent Atomic Orbital Method for NMR Chemical Shift Calculations. *J. Am. Chem. Soc.* **1990**, *112* (23), 8251–8260. DOI: 10.1021/ja00179a005.

Wołowiec, M.; Muir, B.; Zięba, K.; Bajda, T.; Kowalik, M.; Franus, W. Experimental Study on the Removal of VOCs and PAHs by Zeolites and Surfactant-Modified Zeolites. *Energy Fuels* **2017**, *31* (8), 8803–8812. DOI: 10.1021/acs.energyfuels.7b01124.

Xu, X.; Goddard, III W. A. The X3LYP Extended Density Functional for Accurate Descriptions of Nonbond Interactions, Spin States, and Thermochemical Properties. *Proc. Natl. Acad. Sci. U S A.* **2004**, 101 (9), 2673–2677. DOI: 10.1073/pnas.0308730100.

Yang, T.; Dai, F.; Iino, H.; Kanehara, M.; Liu, X.; Minari, T.; Liu, C.; Hanna, J. Solution-Processable Liquid Crystalline Chrysene Semiconductors with Wide Band Gap: Self-Organization and Carrier Transport Properties. *Org. Electron.* **2018**, *63*, 184–193. DOI: 10.1016/j.orgel.2018.09.021.

Yi, P.; Zuo, X.; Liang, N.; Wu, M.; Chen, Q.; Zhang, L.; Pan, B. Molecular Clusters Played an Important Role in the Adsorption of Polycyclic Aromatic Hydrocarbons (PAHs) on Carbonaceous Materials. *Chemosphere* **2022**, *302*, 134772. DOI: 10.1016/j.chemosphere.2022.134772.

Yin, D.-D.; Wu, J.; Xie, C.-B.; Cao Z.-P.; Lü Q.; Zhang, R.-Q. [Comparison of Three-dimensional Fluorescence Characteristics of Two Isomers: Phenanthrene and Anthrancene]. Guang Pu Xue Yu Guang Pu Fen Xi. **2013**, *33* (12), 3263–3268.

Yuan, H.; Tao, S.; Li, B.; Lang, C.; Cao, J.; Coveney, R. M. Emission and Outflow of Polycyclic Aromatic Hydrocarbons from Wildfires in China. *Atmos. Environ.* **2008**, *42* (28), 6828–6835. DOI: 10.1016/j.atmosenv.2008.05.033.

Yue, T.; Lv, R.; Xu, D.; Xu, Y.; Liu, L.; Dai, Y.; Zhao, J.; Xing, B. Competitive and/or Cooperative Interactions of Graphene-Family Materials and Benzo[a]pyrene with Pulmonary Surfactant: A Computational and Experimental Study. *Part. Fibre Toxicol.* **2021**, *18* (1), 46. DOI: 10.1186/s12989-021-00436-9.

Yang, X.; Bittner, E. R. Computing Intramolecular Charge and Energy Transfer Rates using Optimal Modes. *J. Chem. Phys.* **2015**, *142* (24), 244114. DOI: 10.1063/1.4923191.

Zhao, X.-M.; Wei, Y.-K.; Zhang, K.; Zhao, Z.-W.; Wang, S.; Miao, W.; Du, S.-X.; Zhang, S.-J.; Li, W.-F.; Guan, C.-L.; Shi, L.-P.; Lu, X.-P.; Xu, S.-K. Temperature Effect on Vibrational Properties of Crystalline Dibenz[a,h]anthracene. *Spectrochim. Acta A Mol. Biomol. Spectrosc.* **2022**, *274*, 121107. DOI: 10.1016/j.saa.2022.121107.

APPENDIX A. TOTAL ELECTRONIC ENERGY OF PAH MOLECULES

Numbering scheme	PAH molecule	C/H ratio	E_{Total} kcal/mol
1	Naphthalene	1.25	-242159.47
2	Acenaphthylene	1.50	-289972.88
3	Acenaphthene	1.20	-290744.18
4	Fluorene	1.30	-314657.79
5	Anthracene	1.40	-338570.67
6	Phenanthrene	1.40	-338575.81
7	Pyrene	1.60	-386413.66
8	Fluoranthene	1.60	-386399.24
9	Benzo[a]anthracene	1.50	-434988.59
10	Chrysene	1.50	-434990.54
11	Benzo[b]fluoranthene	1.67	-482815.31
12	Benzo[k]fluoranthene	1.67	-482817.25
13	Benzo[a]pyrene	1.67	-482826.67
14	Dibenzo[a,h]anthracene	1.57	-531406.01
15	Benzo[g,h,i]perylene	1.83	-530668.44
16	Indeno[1,2,3-c,d]pyrene	1.83	-530652.63

Table A1: Total electronic energy of the 16 PAHs at the B3LYP/6-31G(d,p) level in gas phase.

APPENDIX B. GAIO CALCULATED NICS VALUE OF PAH MOLECULES AT THE B3LYP/6-31+G* LEVEL

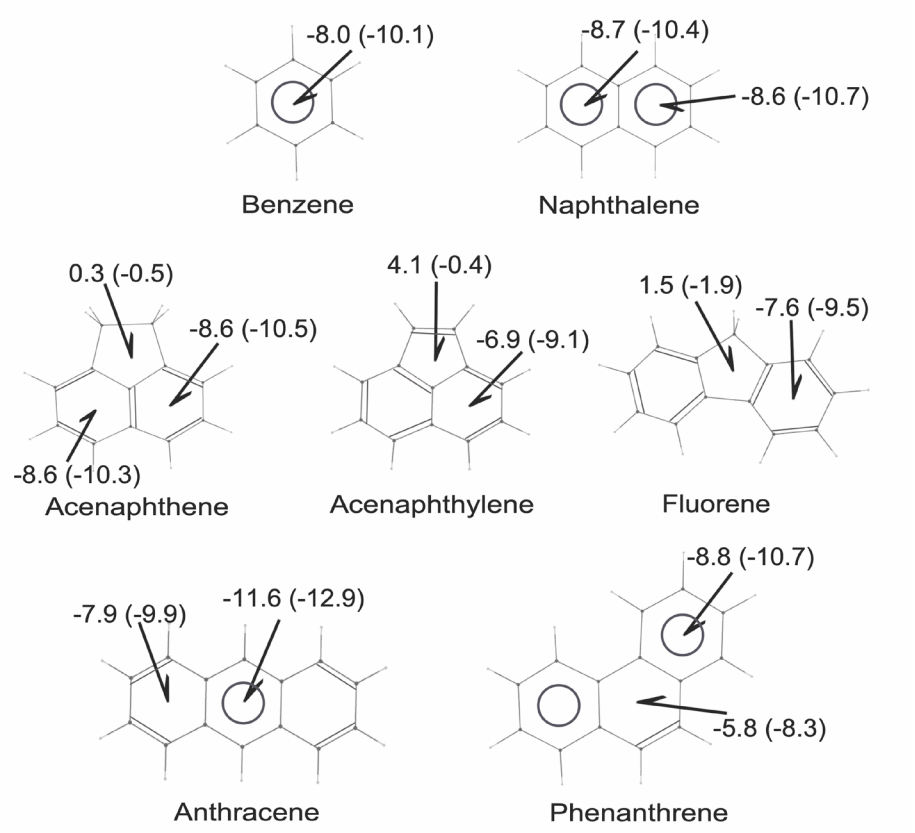

Figure B1: Structures of benzene, naphthalene, acenaphthylene, acenaphthene, fluorene, anthracene, phenanthrene. The NICS(0) at the center of the ring and NICS(1) at a distance of 1 Å above the molecular plane are presented. The NICS(1) value is shown in parentheses. The resonant sextet that is in the center of the ring is shown in circle.

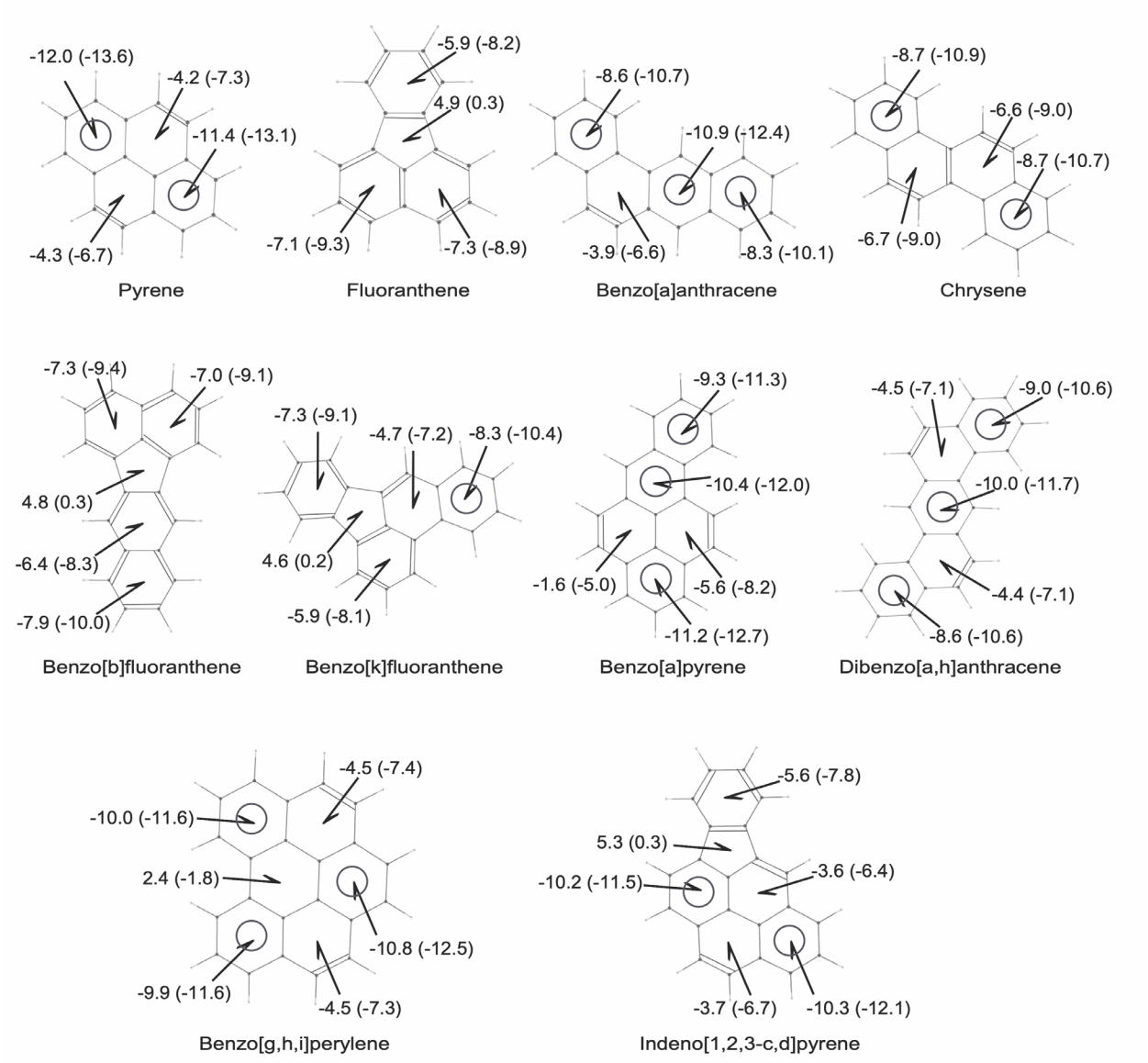

Figure B2: Structures of PAHs with four, five, and six-rings. The NICS(0) at the center of the ring and NICS(1) at a distance of 1 Å above the molecular plane are presented. The NICS(1) value is shown in parentheses. The resonant sextet that is in the center of the ring is shown in circle.

APPENDIX C. THE DENSITY OF STATES (DOS) AND FRONTIER ORBITALS CORRESPONDING TO HOMO AND LUMO OF PAH MOLECULES AT B3LYP/6-31G(D,P) LEVEL

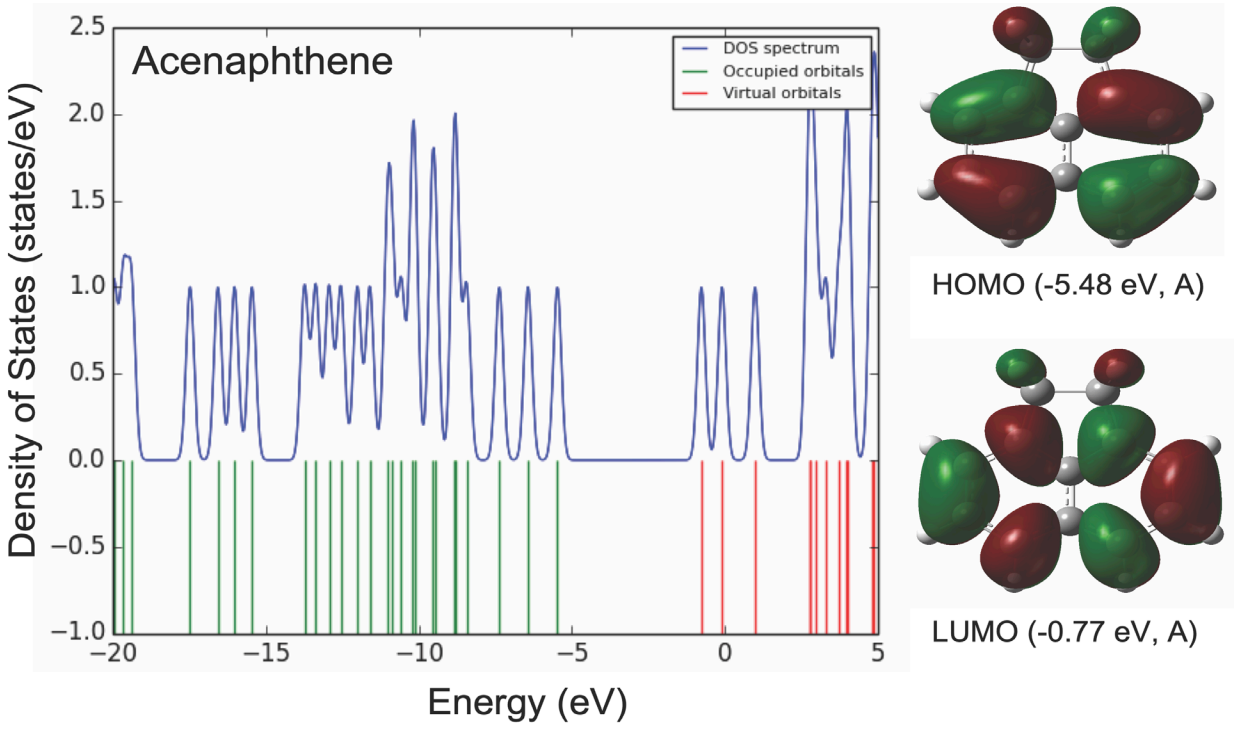

Figure C1: Acenaphthene

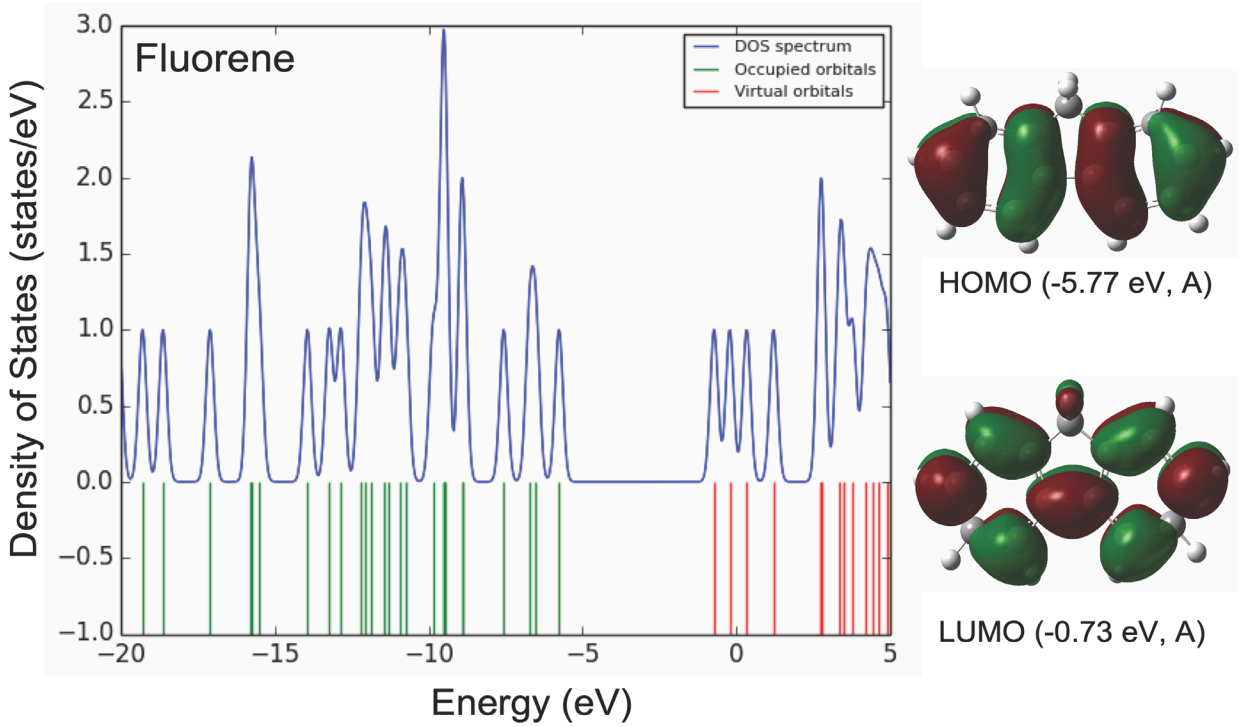

Figure C2: Fluorene

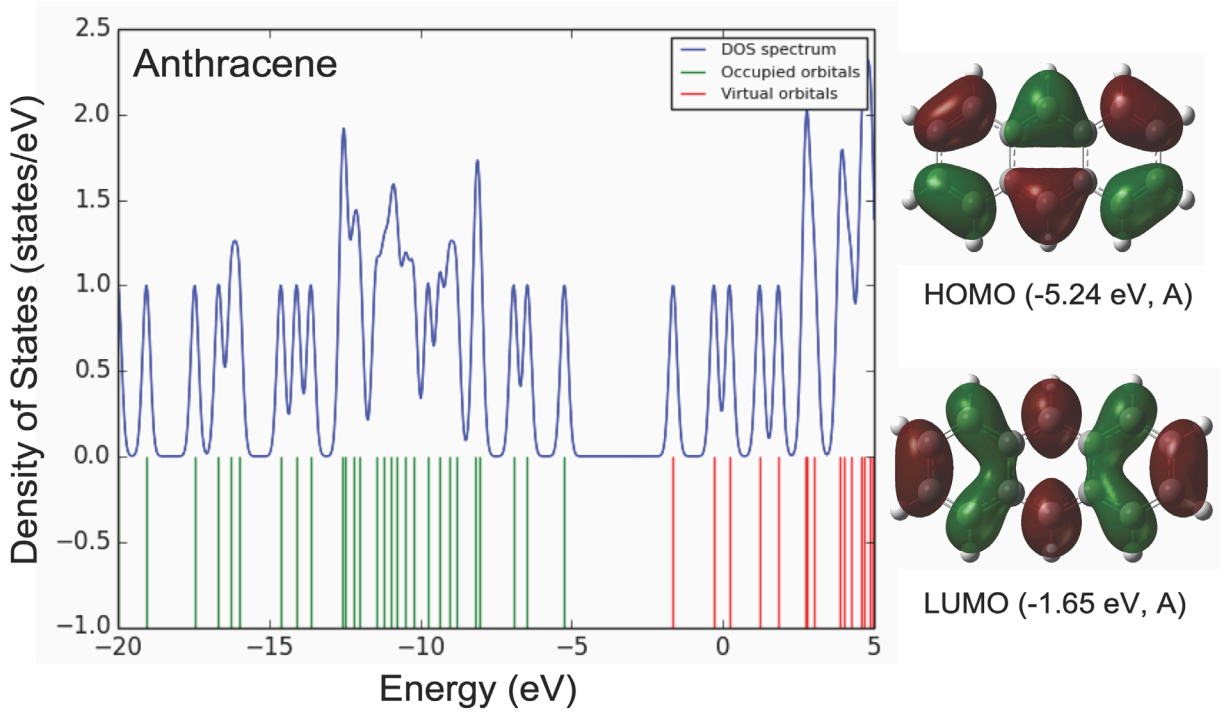

Figure C3: Anthracene

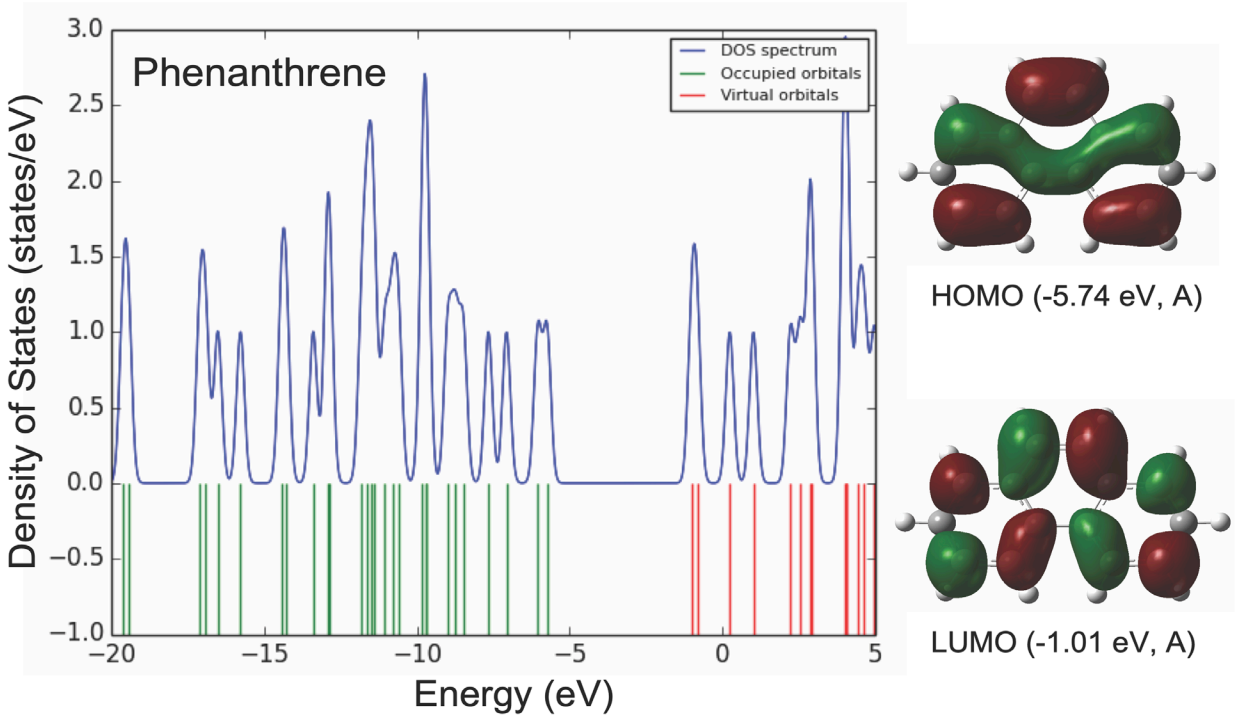

Figure C4: Phenanthrene

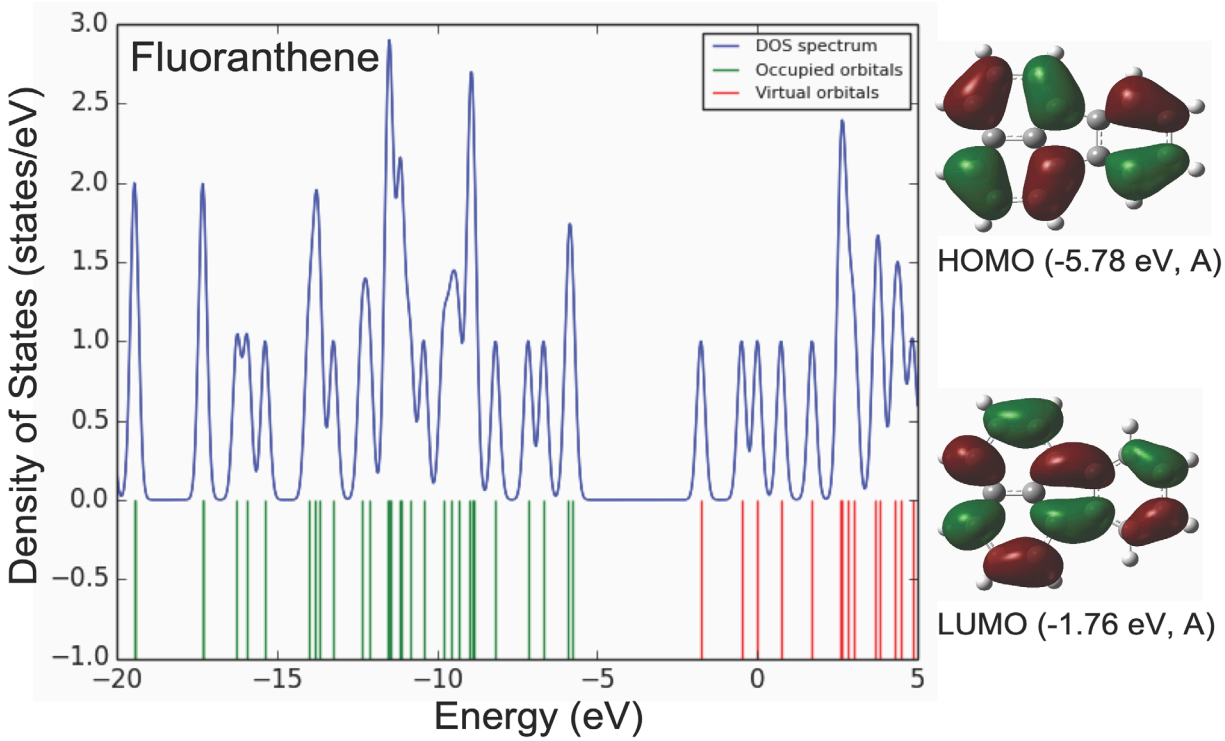

Figure C5: Fluoranthene

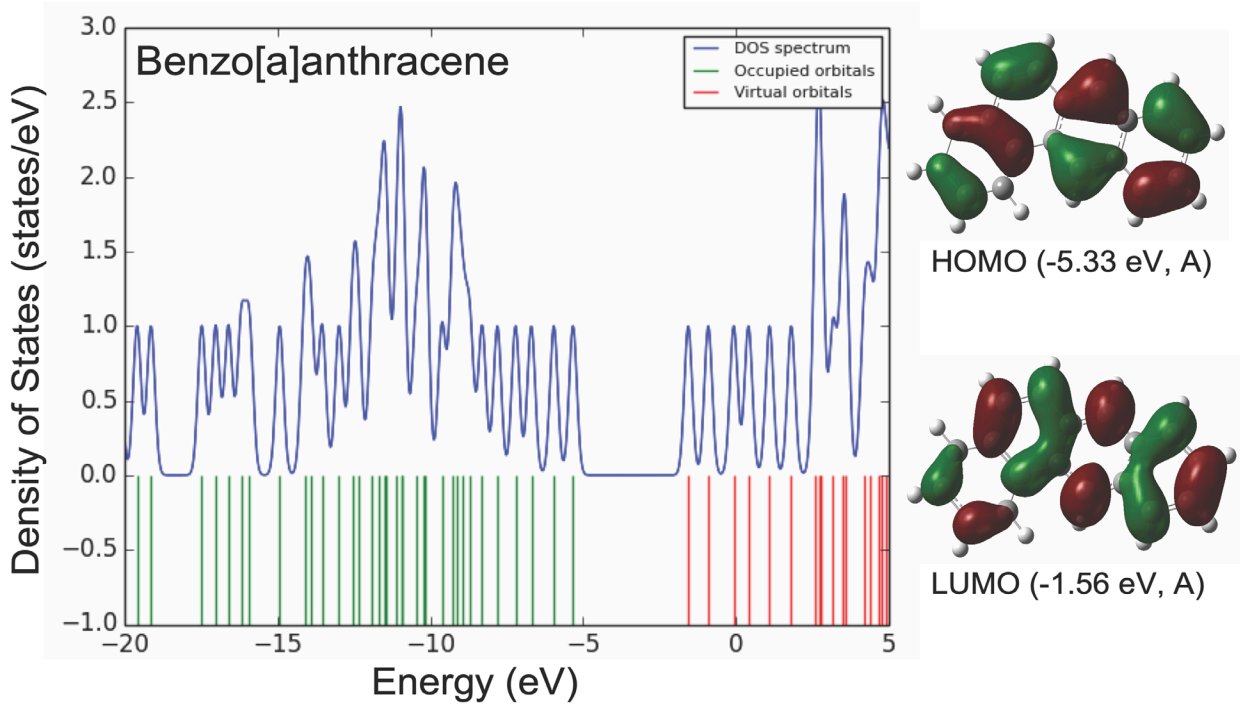

Figure C6: Benzo[a]anthracene

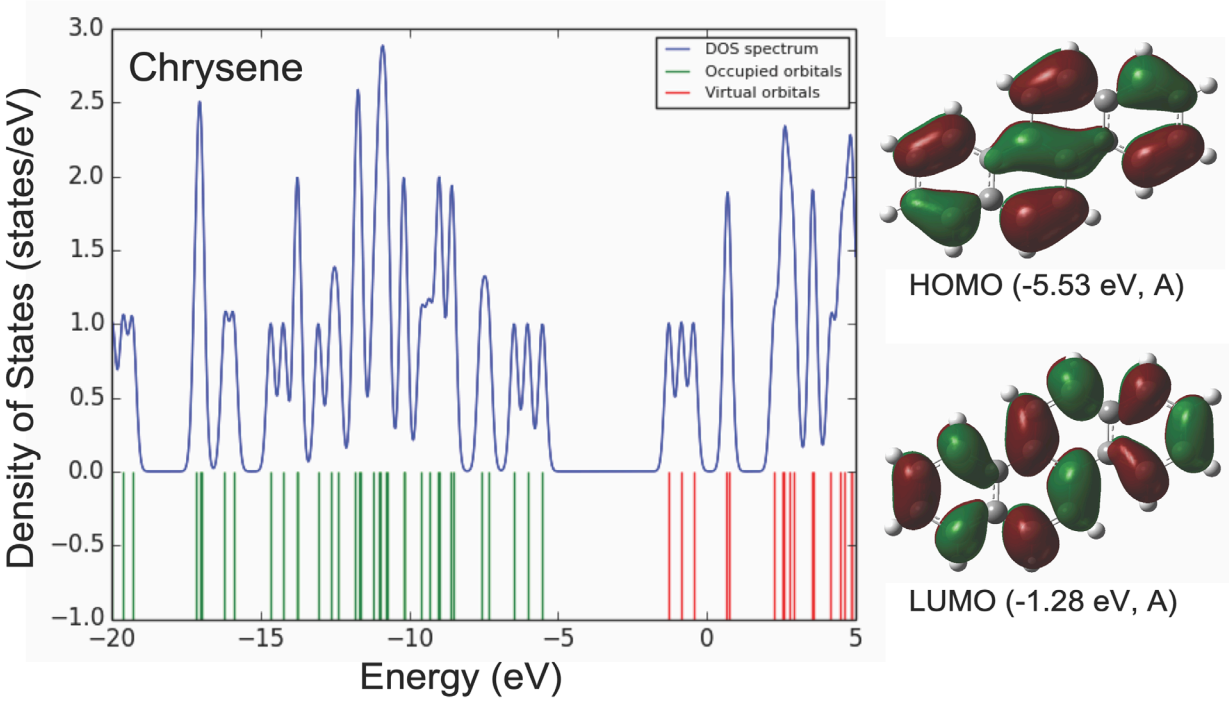

Figure C7: Chrysene

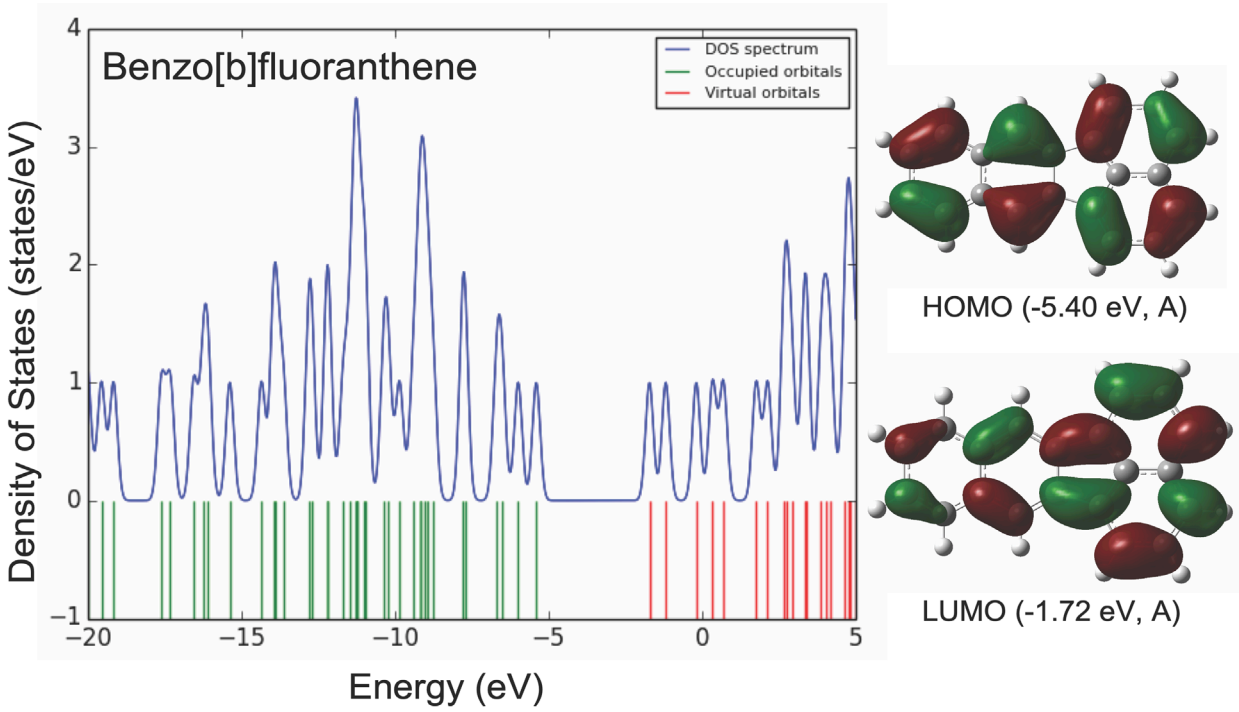

Figure C8: Benzo[b]fluoranthene

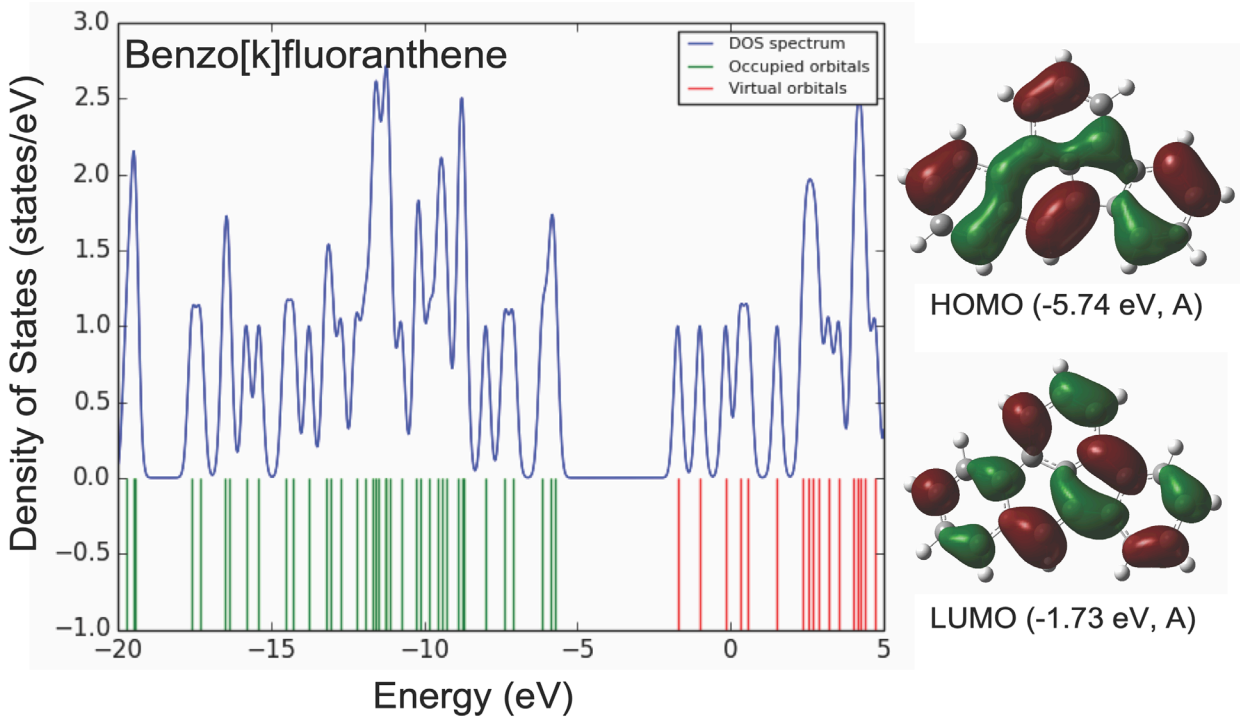

Figure C9: Benzo[k]fluoranthene

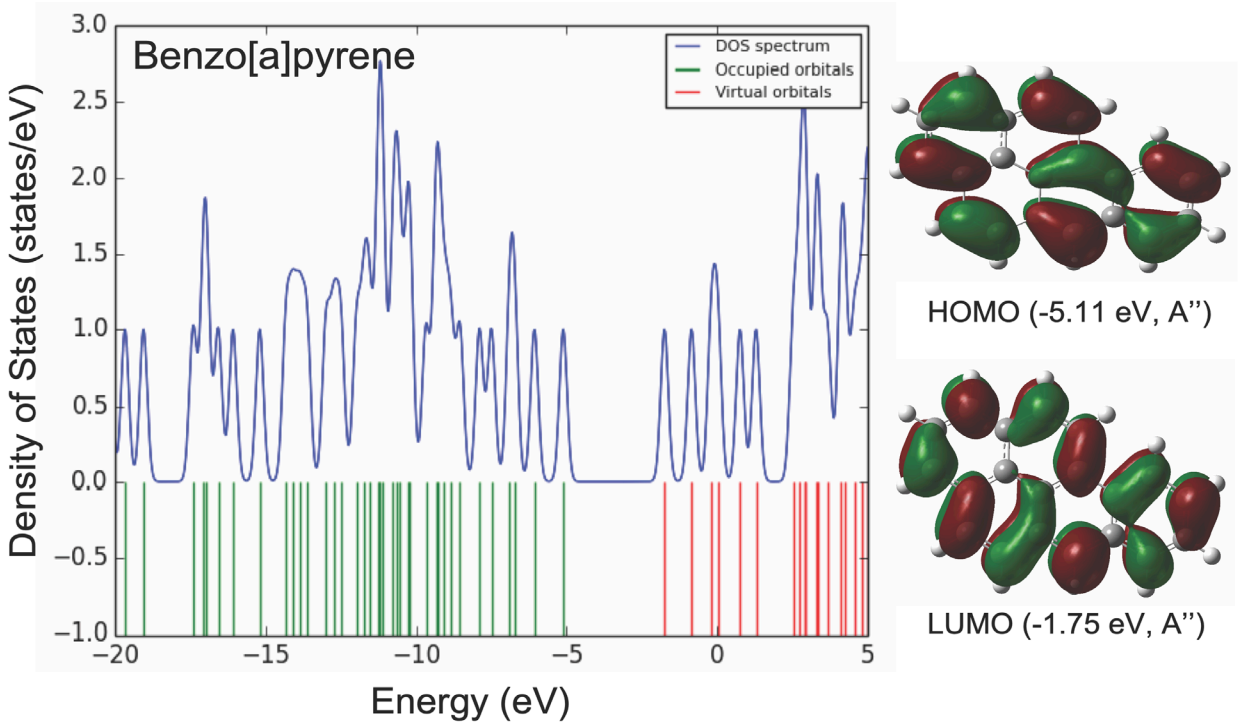

Figure C10: Benzo[a]pyrene

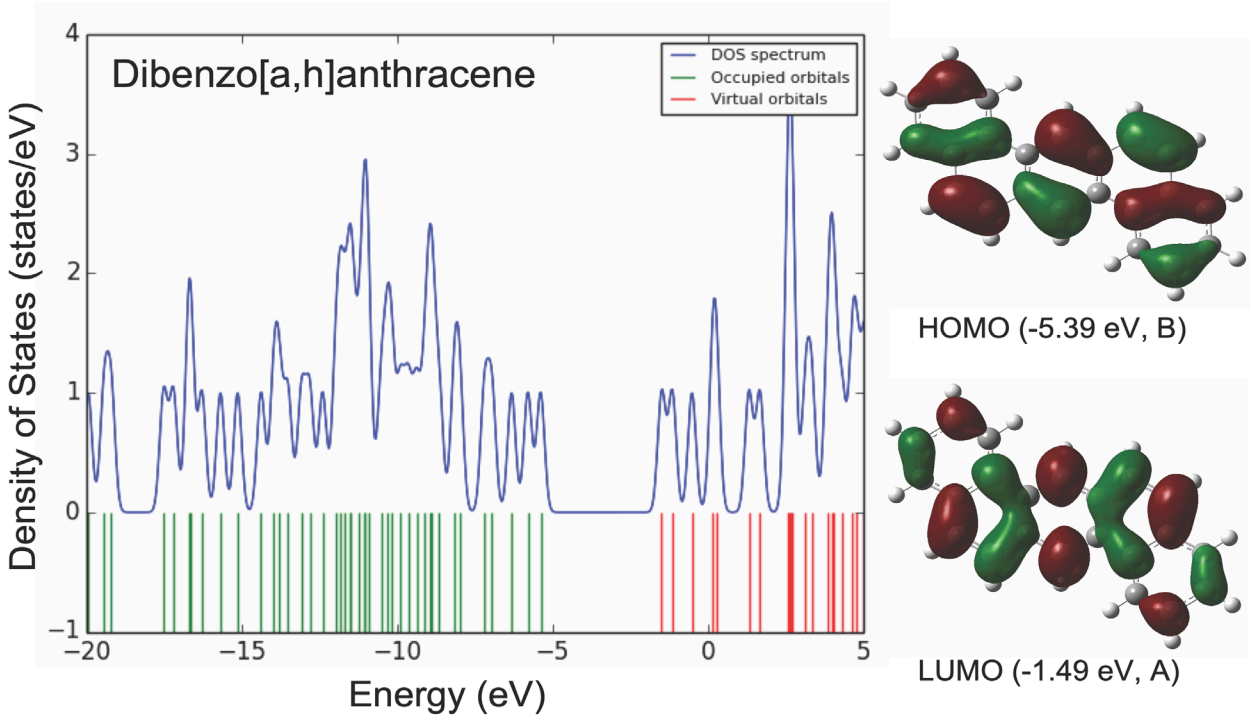

Figure C11: Dibenzo[a,h]anthracene

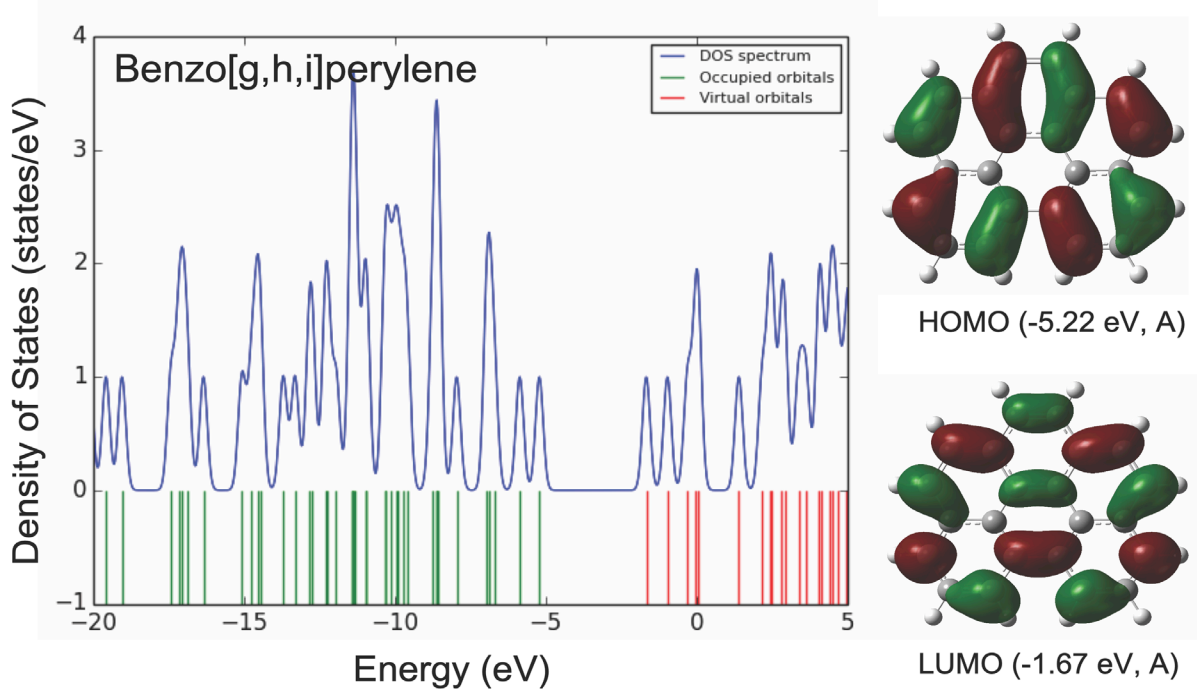

Figure C12: Benzo[g,h,i]perylene

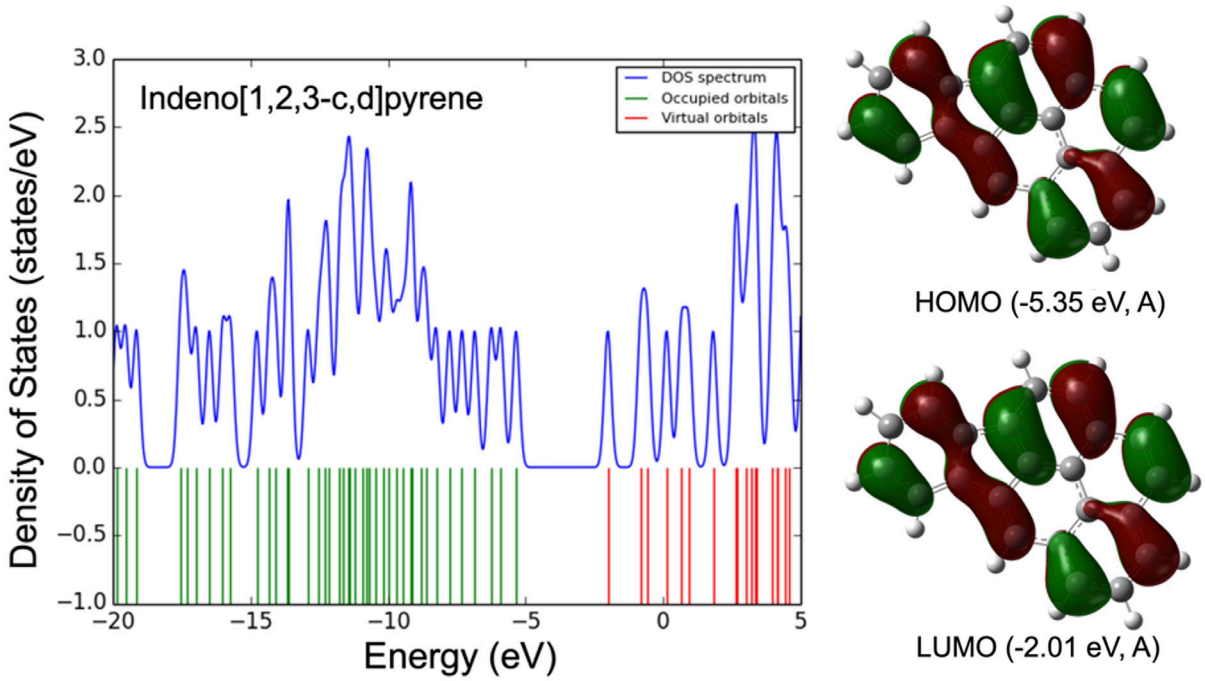

Figure C13: Indeno[1,2,3-c,d]pyrene